Journal of Sedimentary Research

Journal of Sedimentary Research, 2022, v. 92, 487–502
Research Article
DOI: 10.2110/jsr.2021.038

QUANTIFYING RIVER AVULSION ACTIVITY FROM SATELLITE REMOTE SENSING: IMPLICATIONS FOR HOW AVULSIONS CONTRIBUTE TO FLOODPLAIN STRATIGRAPHY IN FORELAND BASINS

JEFFERY M. VALENZA,[1] DOUGLAS A. EDMONDS,[2] AND GARY S. WEISSMANN[3]

[1]*Department of Geography, University of California, Santa Barbara, 1832 Ellison Hall, Santa Barbara, California 93106, U.S.A.*
[2]*Department of Earth and Atmospheric Sciences, Indiana University, 1001 East 10th Street, Bloomington, Indiana 47405, U.S.A.*
[3]*Department of Earth and Planetary Sciences, University of New Mexico, MSC03 2040, Albuquerque, New Mexico 87131, U.S.A.*

ABSTRACT: **The rarely witnessed process of river avulsion repositions channels across floodplains, which influences floodplain geomorphology and stratigraphic architecture. The way avulsions redirect water and sediment is typically generalized into one of two styles. Avulsions proceeding through rapid channel switching and producing little to no floodplain disturbance are annexational, while those that involve sequential phases of crevassing, flooding, and eventual development of a new channel are progradational. We test the validity of these avulsion style categories by mapping and characterizing 14 avulsion events in Andean, Himalayan, and New Guinean foreland basins. We use Landsat data to identify how avulsions proceed and interpret the possible products of these processes in terms of geomorphic features and stratigraphy. We show that during annexation the avulsion channel widens, changes its meander wavelength and amplitude, or increases channel thread count. During progradation, avulsion channels are constructed from evolving distributary networks. Often beginning as crevasse splays, these networks migrate down the floodplain gradient and frequently create and fill ponds during the process. We also see evidence for a recently defined third avulsion style. Retrogradation involves overbank flow, like progradation, but is marked by an upstream-migrating abandonment and infilling of the parent channel. Avulsion belts in this study range from 5 to 60 km in length, and from 1 to 50 km in width. On average, these events demonstrate annexational style over 22.4% of their length. Eleven of 13 events either begin or end with annexation, and seven both begin and end with annexation. Only one event exhibited progradation over the entire avulsion-belt length. While there are many documented examples of purely annexational avulsions, we see little evidence for completely progradational or retrogradational avulsions, and instead suggest that a given avulsion is better envisioned as a series of spatiotemporal phases of annexation, progradation, and retrogradation. Such hybrid avulsions likely produce significantly greater stratigraphic variability than that predicted by the traditional end-member model. We suggest that a time-averaged, formation-scale consideration of avulsion products will yield more accurate characterizations of avulsion dynamics in ancient fluvial systems.**

INTRODUCTION

The natural diversion of river channels, or avulsion, is a rarely witnessed yet formative process in natural floodplains. Avulsion events profoundly impact river-floodplain systems by abandoning previous channels, reactivating old channels, and even building new channels as the river ultimately repositions itself on the floodplain. These large-scale changes in river position affect floodplain geomorphology and build the fluvial stratigraphic record over time (Bridge and Mackey 1993; Kraus et al. 1999; Jones and Hajek 2007) . The relationship between avulsion and fluvial stratigraphy was codified in simplified numerical models ("LAB" models, e.g., Bridge and Mackey (1993)) that showed channel stacking patterns are determined by a variety of factors including channel-belt dimensions and depositional rates, avulsion frequency, tectonic tilting of the floodplain, sediment compaction rates, and variability of overbank deposition. Avulsion directly controls the position of channel belts in a basin, thus indirectly determining the location and timing of other processes associated with channels, such as crevasse splaying (Allen 1965; Burns et al. 2017; Gulliford et al. 2017), levee construction (Brierley et al. 1997; Johnston et al. 2019; Jobe et al. 2020), and alluvial ridge development (Bridge and Leeder 1979; Perez-Arlucea and Smith 1999; van Toorenenburg et al. 2018).

The avulsion process itself can contribute significant quantities of sediment to the floodplain (Smith et al. 1989). This occurs when flow and sediment diverted from the parent channel is not immediately transferred into another channel, but rather redirected out onto the floodplain or fan surface (Smith et al. 1989; Assine 2005; Buehler et al. 2011). As flow spreads and decelerates across the floodplain, significant volumes of sediment can be deposited, resulting in heterolithic sediment packages deposited on top of fine-grained floodplain sediments (Kraus and Gwinn 1997; Kraus et al. 1999; Slingerland and Smith 2004; Jones and Hajek 2007). Thus, avulsions build the floodplain by controlling channel position and hence the stacking pattern (e.g., "LAB" models), as well as depositing significant quantities of sediment on the floodplain as new channels are established (e.g., Smith et al. 1989).

A few important field-scale examples motivate our understanding of avulsion styles and their stratigraphy. First, the 1870s avulsion of the

Published Online: June 2022
 1527-1404/22/092-487

Saskatchewan River in the Cumberland Marshes, Saskatchewan, Canada, transformed more than 500 km^2 of floodplain into a large avulsion belt before reconnecting with the parent channel downstream (Smith and Perez-Arlucea 1994; Smith et al. 1989; Morozova and Smith 1999, 2000; Perez-Arlucea and Smith 1999). The Taquari River, Mato Grosso and Mato Grosso do Sul, Brazil, hosts recent and ongoing avulsions marked by channel bifurcation and extensive overbank flooding across its fan surface (Assine 2005; Porsani et al. 2005; Buehler et al. 2011; Makaske et al. 2012; Louzada et al. 2020). The 2008 Kosi River avulsion on the border of Bihar, India, and southeast Nepal broke through artificial levees and created a flood zone 20 km wide and 100 km long before engineers redirected flow back to its previous course (Sinha 2008, 2009; Chakraborty et al. 2010).

Considering these examples, along with insights from the stratigraphic record, avulsion events are usually divided into two general styles based on how the avulsion shifts the channel to a new location on the floodplain (Smith et al. 1989; Brizga and Finlayson 1990; McCarthy et al. 1992; Richards et al. 1993; Kraus et al. 1999; Slingerland and Smith 2004; Jones and Hajek 2007). Cases like the Saskatchewan, Taquari, and Kosi River avulsions divert flow out of the parent channel and onto the adjacent floodplain, typically generating a crevasse-splay complex. As the complex advances, or progrades, across the floodplain or fan a single, dominant flow path coalesces from the distributary network to form a new primary channel (Smith et al. 1989; Slingerland and Smith 2004). Eventually, these progradational avulsions reconnect to a downstream reach of the parent channel or an adjacent channel system. Alternatively, annexational avulsions divert flow directly into pre-existing channels with little to no floodplain disturbance (Slingerland and Smith 2004; Flood and Hampson 2014; Edmonds et al. 2016; Valenza et al. 2020).

The historic paucity of field-scale avulsions observed in real time makes it difficult to determine how closely avulsions fall into either annexational or progradational end members. Data were typically derived from either single events, channel maps from before and after avulsion, or snapshots of an ongoing event. For example, historical records dating back hundreds of years document avulsing channels in the Rhine–Meuse Delta (Stouthamer and Berendsen 2001) and rivers draining the Nepalese and Indian Himalaya (Gole and Chitale 1966; Bristow 1987; Mitra et al. 2005; Chakraborty et al. 2010), but it is unclear how the channels avulsed. Similarly, numerous avulsion events documented in the literature focus on surficial sedimentary evidence, historical maps, or shallow core sampling (Yellow River (Xue 1993); Columbia River (Makaske et al. 2002); Rhine–Meuse Delta (Stouthamer 2001; Stouthamer and Berendsen 2001); Kosi River (Sinha 2009); Niobrara River (Ethridge et al. 1999); Sarda River (Mitra et al. 2005); Rio Colorado (Donselaar et al. 2013); Taquari River (Assine 2005)). Since many of these avulsions were not measured in action, we have a limited understanding of what happens during the avulsion event. Creating a dataset of avulsions in action allows us to identify and quantify the processes involved. Practically, this will improve our ability to interpret and predict the arrangement and composition of fluvial avulsion stratigraphy, and conceptually this will allow us to evaluate the annexational–progradational end-member model of avulsion style.

The sedimentary record has largely been the source of data about river avulsions, but recent work highlights the power of the remote-sensing record (Edmonds et al. 2016; Lombardo 2016; Valenza et al. 2020). These studies have identified more than 60 avulsions from the Landsat record. Valenza et al. (2020) identified and tracked avulsion-related floodplain disturbance for 63 events in Andean, Himalayan, and New Guinean foreland basins (Fig. 1). Here, we examine 14 of these avulsions in greater detail to test and refine conceptual models of avulsion style. Thirteen of them demonstrate significant progradational activity, and we evaluate how activity evolves through space and time. For comparison we include one exclusively annexational event. We quantify the style of avulsion events by identifying the avulsion activity along each avulsion belt through space and time. We identify annexational and progradational activity along the avulsion belt, and a newly described avulsion process termed retrogradation (Edmonds et al. 2022). Mapping avulsion activity reveals the processes through which avulsions proceed across the floodplain. We then use these data to discuss how avulsions likely contribute to floodplain sedimentation and the potential avulsion-related facies they might produce.

METHODS

Remote Sensing

To understand how avulsions proceed in space and time, we follow Valenza et al. (2020) and create time-transgressive maps of avulsion-related floodplain activity, which we refer to as avulsion fingerprints. To create each fingerprint, we apply a four-step process to Landsat data from 1986 to 2017 (missions 5, 7, and 8) using Google Earth Engine (Fig. 2). First, we create an annual composite for each avulsion site by applying a median reducer to all available Landsat imagery for a given year. This creates a single image that represents the median spectral conditions for that year (Fig. 2A). Next, on each annual composite, we apply the Tasseled-Cap Transformation (TCT) (Kauth and Thomas 1976; Crist and Cicone 1984; Crist 1985; Crist and Kauth 1986; Huang et al. 2002; Baig et al. 2014), which transforms Landsat bands into physically meaningful spectral bands representing brightness, greenness, and wetness (Fig. 2B). We define avulsion activity in each TCT image by applying three thresholds—we select those pixels with greenness values below the median for the image, and with either brightness values at or above the 90th percentile, or wetness values at or above the 75th percentile. Pixels that satisfy these conditions indicate channel and avulsion-related floodplain activity (Fig. 2B), as validated by Valenza et al. (2020), because avulsions tend to cause flooding (high wetness), which kills vegetation (low greenness) or deposits fresh sediment (high brightness). This creates a single-year avulsion fingerprint, which is a binarized map of avulsion activity. The fourth and final step is to flatten all yearly fingerprints into a final time-transgressive fingerprint of avulsion activity (Fig. 2C). In this study, we discretize avulsions in time by analyzing sequential yearly activity, and in space by analyzing total activity at regular intervals along the avulsion belt.

Dataset of River Avulsions

Our dataset of river avulsions is drawn from the 63 avulsion events in Andean, Himalayan, and New Guinean foreland basins described by Valenza et al. (2020). For each event, Valenza et al. (2020) calculated an avulsion style ratio (S_R), defined as the total area of all avulsion activity pixels identified in the final composite fingerprint (A_T) relative to the surface area of the parent channel (A_P):

$$S_R = \frac{A_T}{A_P} \quad (1)$$

Both A_T and A_P are measured over the whole avulsion belt from the initiation site to where the avulsion rejoins the parent channel or an adjacent channel system. Valenza et al. (2020) found that 50 of the 63 avulsions were purely annexational with $S_R < 2$. This means that there is minimal floodplain disturbance associated with the avulsion. In this paper, we analyze in detail the remaining 13 with $S_R > 2$ because those events are likely more important for floodplain building and sediment deposition. For comparison, we add one example (H5) with $S_R < 2$ to compare a purely annexational avulsion with the other events.

Characterizing Variation in Avulsion Style

To characterize the variation of style within each avulsion, we discretize events in space and time. To characterize spatial variability, we compare

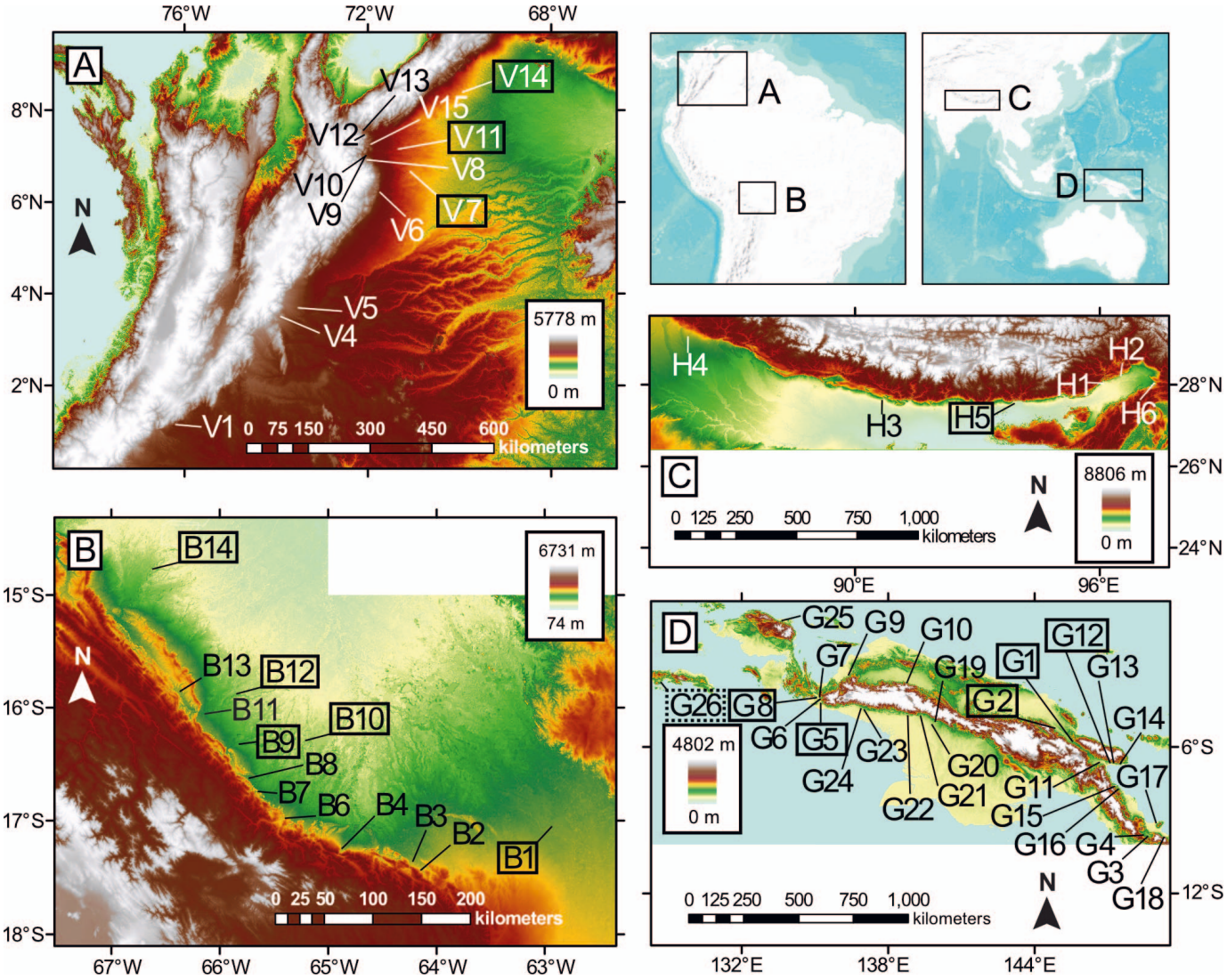

FIG. 1.—Locator map of all avulsion events presented by Valenza et al. (2020). Events are in northern and central Andean, central to eastern Himalayan, and various New Guinean foreland basins. We focus on events that demonstrate at least some progradation, which are highlighted by black boxes around sample numbers. Sample H5, an exclusively annexational event, is included in all analyses for comparison. Sample G26 is shown to the west of New Guinea and is used to demonstrate an ideal example of single-thread, gradual annexation (Fig. 4) but is otherwise not analyzed in this study.

localized avulsion activity along the channel belt to the background, or characteristic activity of the parent channel. To do this, we place nodes along the avulsion channel-belt centerline at intervals equal to ten times the parent-channel width (except avulsions G5, G12, and H5, for which nodes are placed at intervals exactly equal to the parent-channel width). We then assign all avulsion pixels to their nearest node and count the number of pixels per node (A_N) (Fig. 3). Using pre-avulsion Landsat imagery, we repeat this discretization along the imminent abandonment reach of the parent channel. We then count the number of active channel pixels for each parent-channel node and take the average of these node counts to estimate a characteristic parent-channel area ($\overline{A_P}$). Finally, we compare A_N to $\overline{A_P}$ to calculate a nodal avulsion style ratio (S_{RN}).

$$S_{RN} = \frac{A_N}{\overline{A_P}} \quad (2)$$

We calculate S_{RN} from both yearly avulsion fingerprints (Fig. 2B) and final composite fingerprints (Fig. 2C). Using composite fingerprints, we lose temporal resolution but identify the maximum avulsion extent at each node. Using yearly fingerprints, we track the progression of avulsion activity through time. To do this, we identify the center of yearly avulsion activity, defined as the center of mass of avulsion activity for a given year, assuming a unit mass of deposition for all activity pixels. To calculate the center of avulsion activity, we give a sequential value to nodes, weight them with respect to S_{RN}, and find the average location. We also calculate the yearly average S_{RN} and consider it graphically with the center of avulsion activity.

S_{RN} is similar to S_R except that it is calculated at individual nodes instead of the entire avulsion belt at once. Using high-resolution imagery, Valenza et al. (2020) found that avulsions with $S_R < 2$ have avulsion activity that is roughly equal to the parent-channel surface area, which suggests that the new avulsion channel behaves similarly to the parent channel. We find that annexation thresholds for S_{RN} are slightly higher because the node-based calculation of activity area is more sensitive to channel migration.

We choose the annexational cutoff of $S_{RN} < 3$ because in avulsion B9, for example, the first reach of the river is clearly annexational but yields

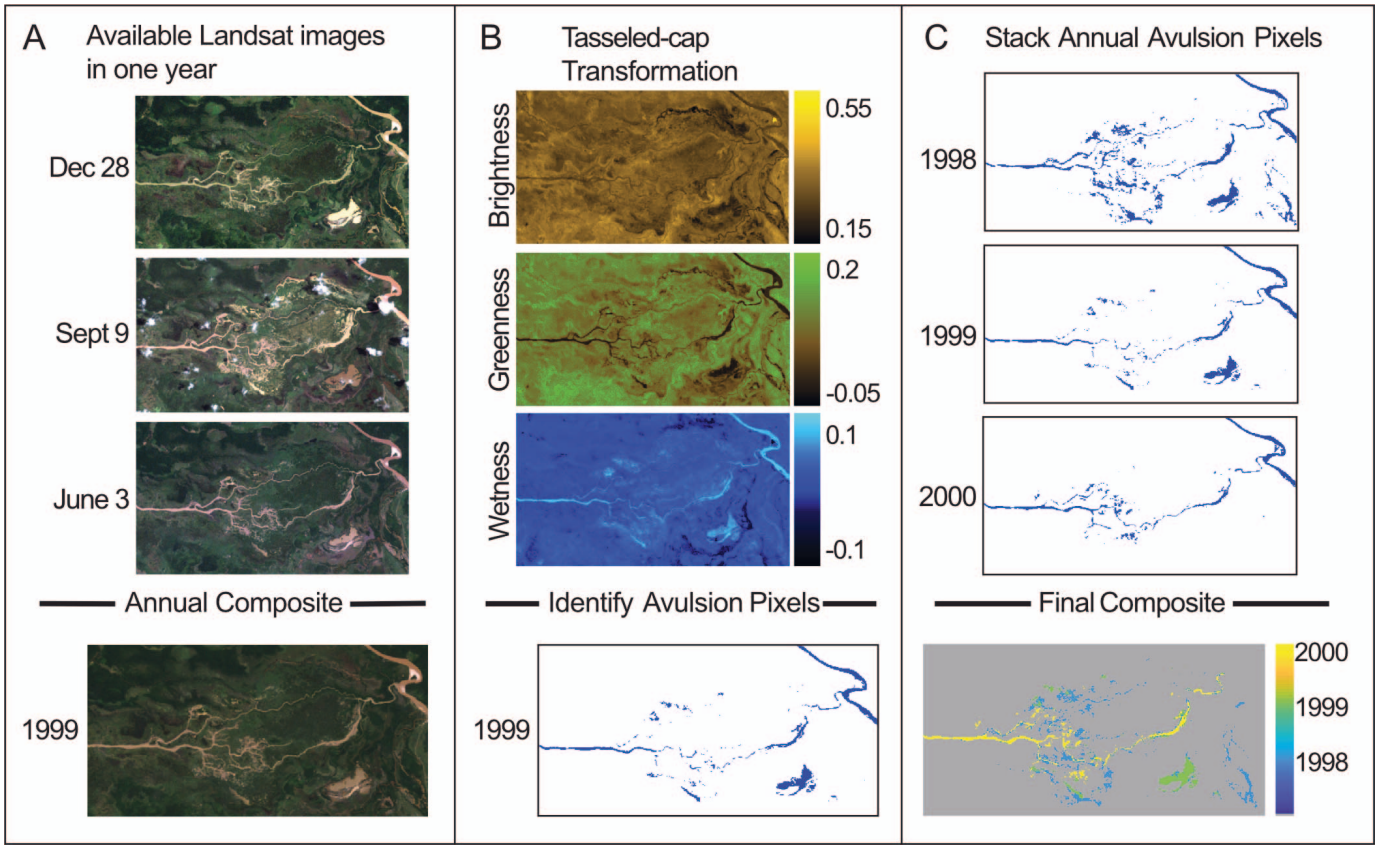

FIG. 2.—Creating avulsion fingerprints requires three steps: **A)** Apply a median reducer to all images in each year to obtain an annual composite. Note that there are usually many more than three images in a year. **B)** Apply a Tasseled-Cap Transformation of the annual composite to compress all Landsat bands into three new bands (following methods described by Crist and Cicone (1984) and Crist and Kauth (1986)) that represent brightness, greenness, and wetness. We then apply empirically derived thresholds from Valenza et al. (2020) to identify the avulsion-related pixels. This creates a single-year avulsion fingerprint. **C)** We take all single-year avulsion fingerprints and compress them into a final time-transgressive composite fingerprint. Avulsion sample V11, Venezuela, 7.170367° S 71.345822° W.

S_{RN} values between 2 and 3 (avulsion B9 is discussed in detail in the section titled, "How do the various avulsion processes interact?"). For the purposes of this study, we assume that an $S_{RN} < 3$ represents reoccupation of pre-existing channels, incision of new channels, or avulsion activity below temporal or spectral resolution. We refer to these processes as annexation. Nodes with $S_{RN} > 3$ contain observable floodplain activity and are classified as progradational nodes. We first consider the maximum extent of avulsion activity, using S_{RN}, which counts all pixels that demonstrated activity at least once in the course of the avulsion at a given node. We then consider the average value of S_{RN} for all nodes for a given year (for discussion of both uses of S_{RN}, see Results).

RESULTS

For the 14 avulsions analyzed in this study, we identified and defined distinct processes that comprise each event based on whether avulsion activity was focused in channels or on floodplains, and whether floodplain activity progressed up or downstream. We quantified this activity by calculating S_{RN} along the length of the avulsion belt and interpreted the dominant process for a given reach based on the magnitude of S_{RN} and the migration direction of avulsion activity. We classified nodes on the avulsion channel with $S_{RN} < 3$ as annexational, nodes with $S_{RN} > 3$ that show downstream activity migration as progradational, and nodes with $S_{RN} > 3$ that show upstream activity migration as retrogradational. Following Valenza et al. (2020), we assume that avulsion activity identified in each remote-sensing scene represents a combination of flooding, vegetation die-back, and sedimentation during the avulsion.

Annexation

We find that annexation typically occurs when the parent channel migrates laterally into a pre-existing channel, overbank flow is captured by a pre-existing channel, or when headward erosion of incipient avulsion channels capture parent-channel flow. During the process of annexation, the channel capturing the flow must adjust to the new water and sediment discharge. Occasionally, the annexed channel can accommodate the flow with minimal change, but this seems rare. Instead, if the annexed channel is too small, then it may widen (Fig. 4), increase its number of channel threads (Fig. 5), or change meander amplitude and wavelength (see treatment of avulsion B9). In one case where the avulsion occurs on a single-thread river (avulsion G26), a small part of the flow is diverted into a local drainage channel. The annexed channel widens over 16 years as the parent channel is completely diverted (Fig. 4). In another case on a multithreaded river (avulsion H5), annexation begins with the diversion of a single thread from the parent braid belt to a relict braid belt in 1989. Over time more threads migrate to the relict braid belt, and by 2012 the avulsion is complete, and the width of the annexed braid belt is comparable to the parent's width before avulsion (Fig. 5). Channel widening may be common when the avulsing channel annexes a smaller floodplain drainage channel. Annexation of a relict channel of similar scale to that of the parent channel,

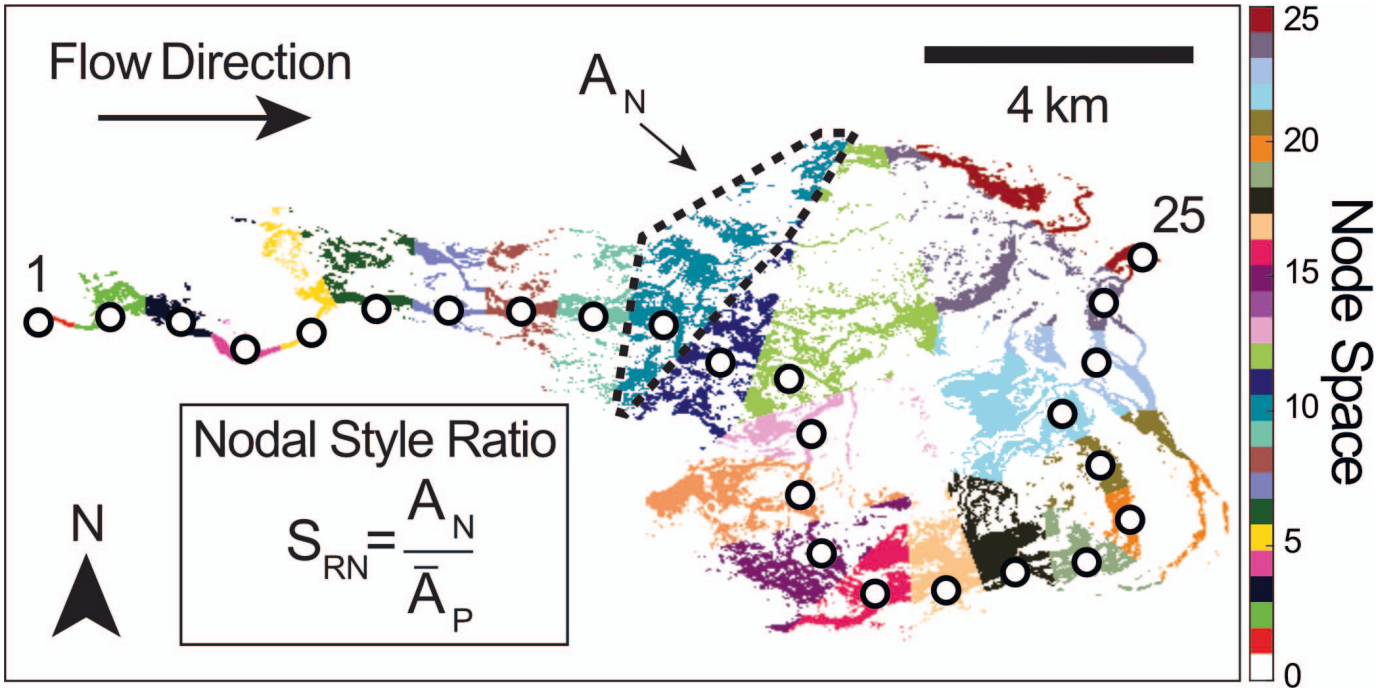

FIG. 3.—Calculation of nodal avulsion style ratios (S_{RN}). Nodes (black-lined circles) are placed at intervals scaled to the width of the parent channel along the final avulsion channel-belt centerline, where the first and last nodes are marked by "1" and "25," respectively. Each avulsion fingerprint pixel is assigned to the nearest node, here represented by different colors. The area of those pixels for a given node is A_N. A similar process is repeated on the parent channel, but all nodes are averaged to get $\overline{A_P}$. Avulsion sample V11, Venezuela, 7.170367° N 71.345822° W.

such as an abandoned channel of the same primary system, likely results in minimal channel width adjustment as the annexed channel can generally accommodate the new flow volume. As we show later, when the annexed channel cannot transport the sediment and water from the parent channel, the avulsion transitions into a phase of progradation or retrogradation.

Progradation

Progradational avulsion activity proceeds from single-thread channels and usually begins as a crevasse splay (Valenza et al. 2020). Once flow is diverted from the parent channel, the avulsion progrades downstream

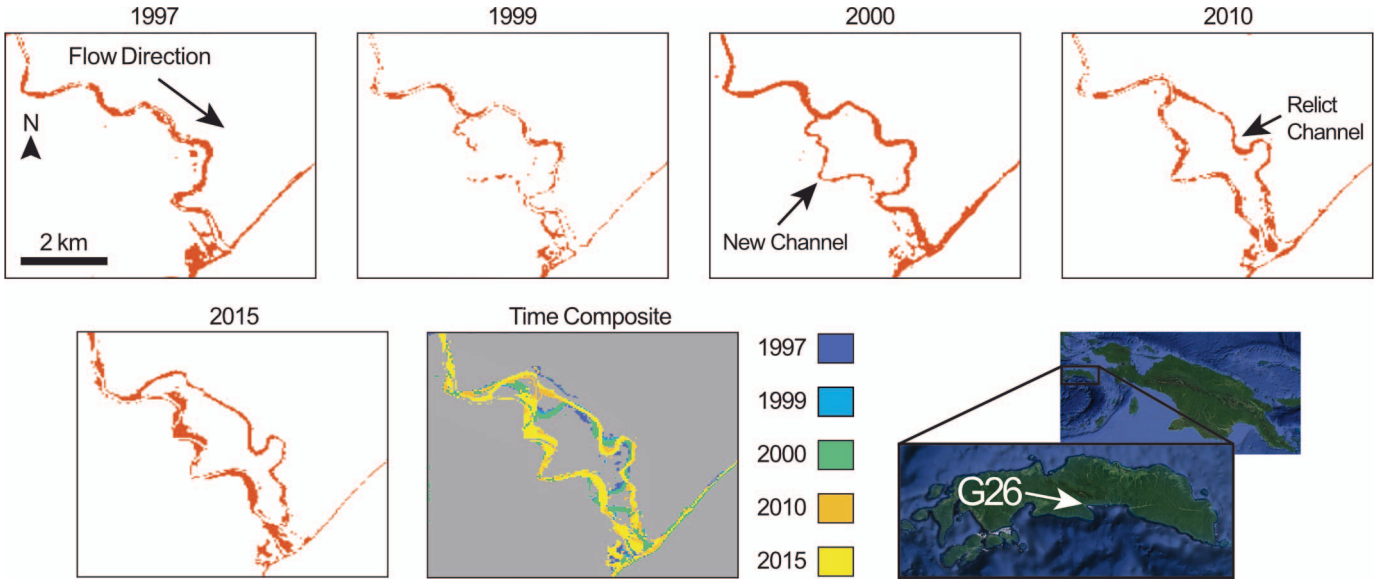

FIG. 4.—Example of a single-thread river avulsing through annexation over time. The time composite panel shows sum of yearly activity as a flattened image. Note that this event was processed using surface brightness and greenness thresholds, so that channel sediments, not water, are used for detection of avulsion activity. In cases where the wetted channel width was smaller than Landsat resolution (30 m) we turned to surface brightness to visualize floodplain disturbance. In this case, the abandoned channel remains visible as bare sediment. Flow direction (FD) is indicated by arrow. Avulsion sample G26, Indonesia, 3.317258° S 128.6812° E.

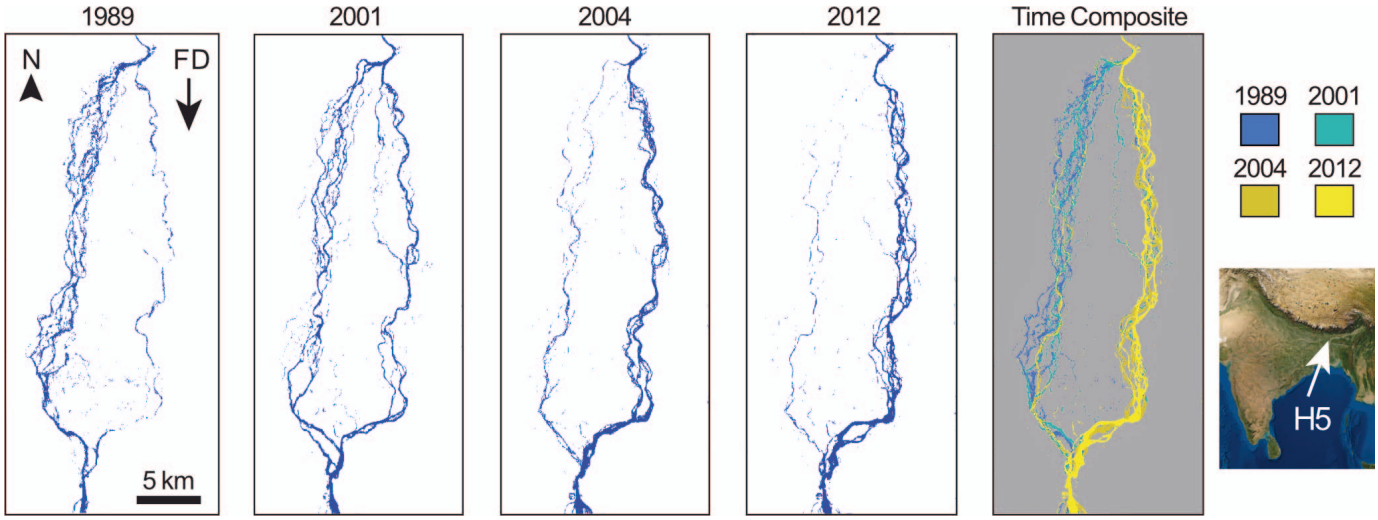

FIG. 5.—Example of a multi-thread river avulsing through annexation. The time composite panel shows sum of yearly activity as a flattened image. Note that flow shifts thread by thread until the greater part is transferred from the western to the eastern braid belts. Flow direction (FD) is indicated by arrow. Avulsion sample H5, India, 26.7838° N 90.956467° E.

through evolving distributary channel networks (Fig. 6). Eventually, flow is concentrated into a new channel, abandoning the others, in a similar manner to that described by Smith et al. (1989) in the Saskatchewan River avulsion. In some cases, the avulsion progrades into ponded water, which is then partially or completely filled (Figs. 7, 8). In these cases, delta deposition fills the pond.

During progradation, avulsion activity is not always channelized. In fact, the most laterally extensive activity we observe is nonchannelized flow (Fig. 8). This activity is the result of the diversion of flow away from the parent channel and out onto floodplain areas that are not efficiently drained by existing channels. Without a new channel to provide efficient transport, nonchannelized activity occurs across low-relief areas of the floodplain, and lasts only until other processes take effect.

Retrogradation

Retrogradational avulsions were recently defined and described by Edmonds et al. (2022). Retrogradational avulsion activity differs from progradation in two important ways. First, diverted flow fails to form significant distributary networks or new channels, mainly resulting in short-lived, nonchannelized flow or ponding. Second, the avulsion initiation site migrates upstream along the parent channel, as opposed to the fixed initiation site typically seen in annexation or progradation. It is not clear what initiates retrogradation, but Lombardo (2017) and Edmonds et al. (2022) suggest some kind of channel blockage (e.g., a log jam) is required. In two examples, it appears that the annexed channel is too small to transport the new discharge, resulting in multiple short-lived crevasse splays or zones of nonchannelized flow, and a phase of retrogradation occurs as the activity migrates upstream over time (Figs. 9, 10). It appears

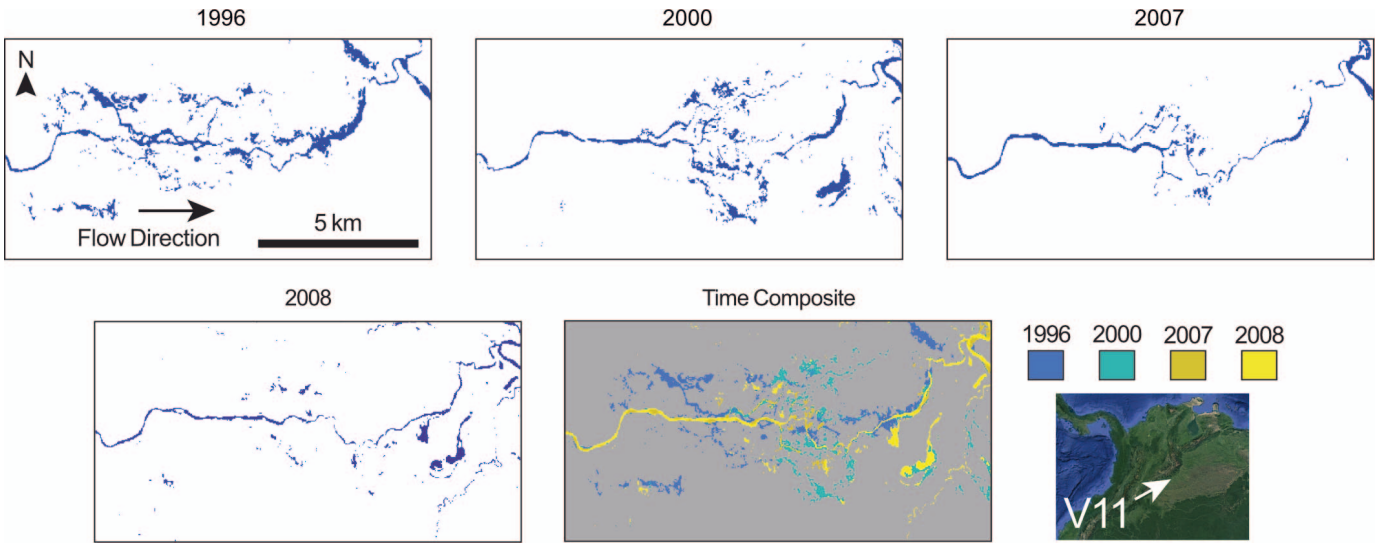

FIG. 6.—Example of a prograding distributary network. By year 2008, the distributary network has nearly coalesced into a single channel. The time composite panel shows sum of yearly activity as a flattened image. Avulsion sample V11, Venezuela, 7.170367° N 71.345822° W.

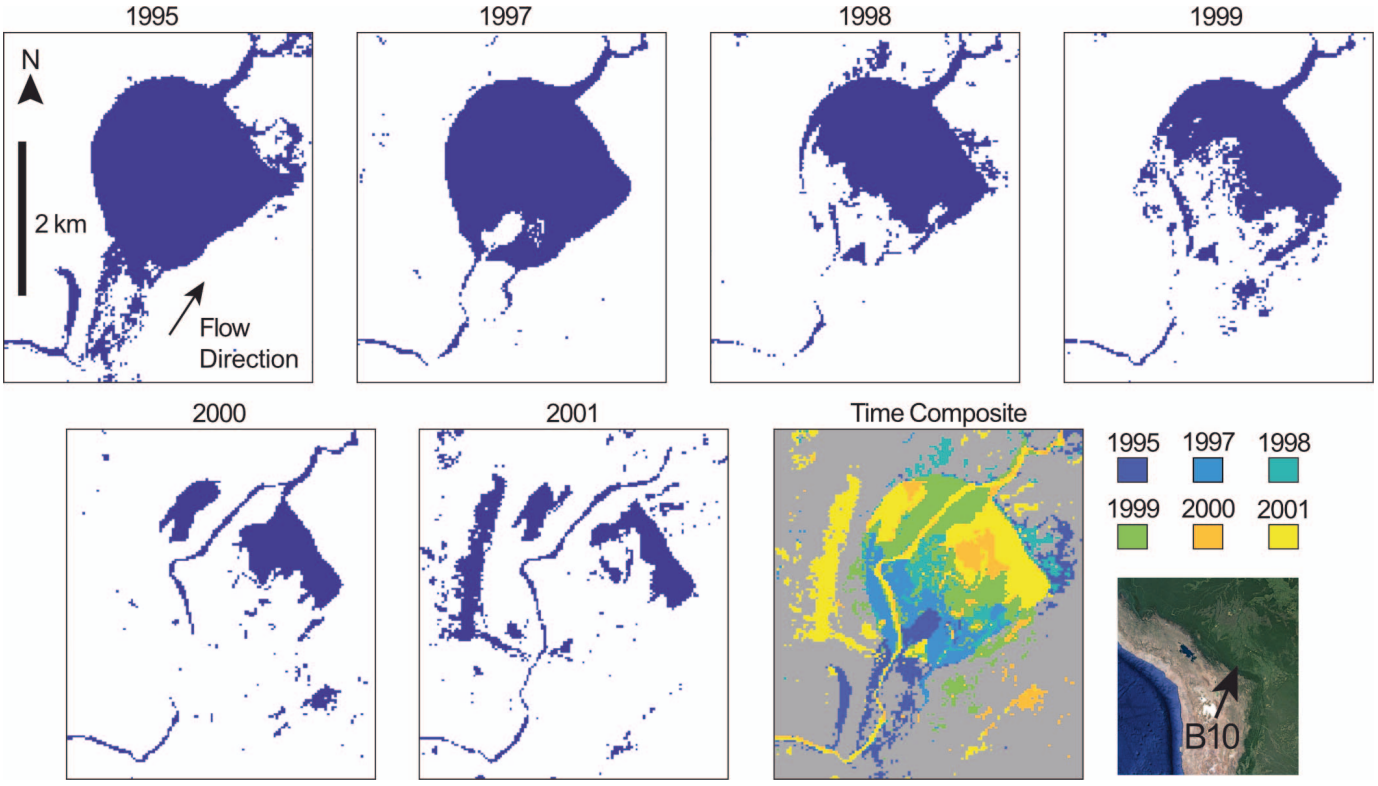

FIG. 7.—Example of delta formation and lake fill during channel progradation over time. The time composite panel shows sum of yearly activity as a flattened image. Avulsion sample B10, Bolivia, initiates at 16.272997° S, 65.203928° W, and the location of this lake fill is 16.250901° S, 65.137224° W. See Supplemental Figure 1 for Landsat image progression for this process.

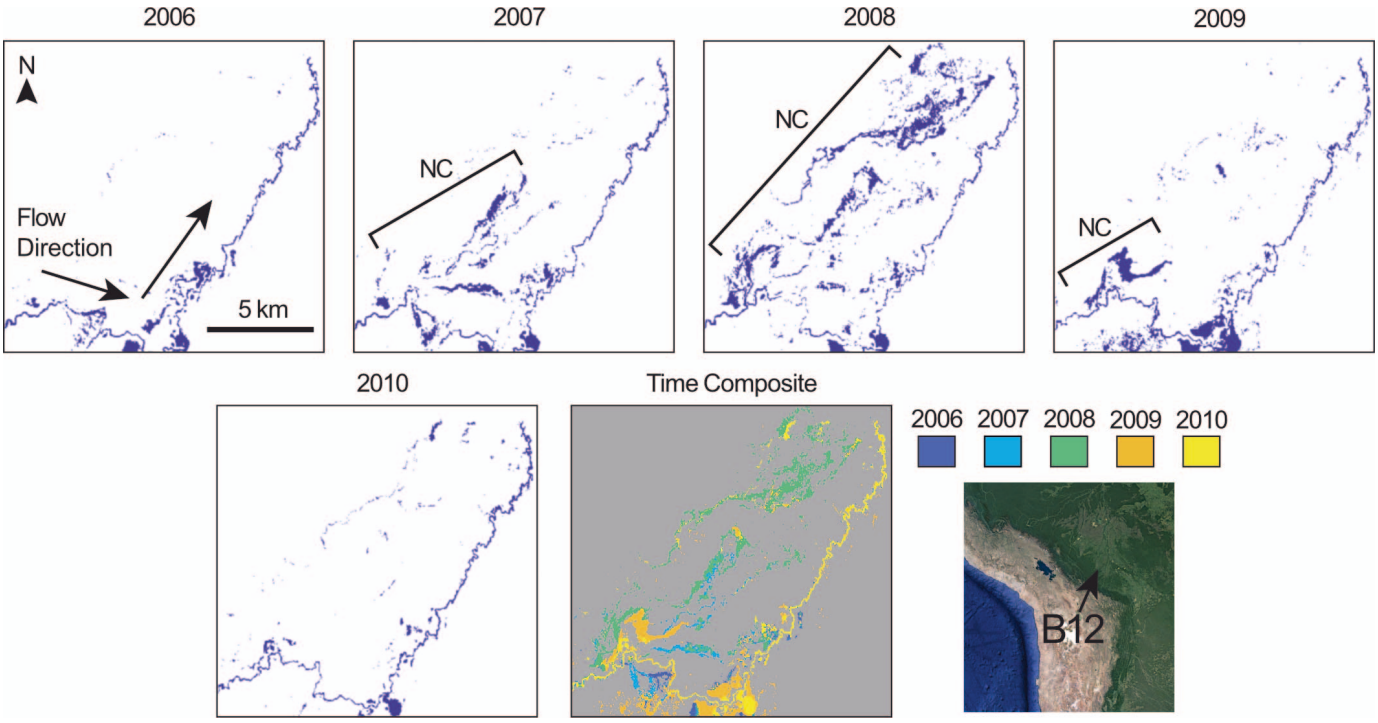

FIG. 8.—Example of nonchannelized flow (NC) emanating from an avulsion network over time. The time composite panel shows sum of yearly activity as a flattened image. This process is short-lived. Starting in 2007, nonchannelized flow extends over 10 km on the floodplain parallel to the annexed channel, before ceasing by 2010. Avulsion sample B12, Bolivia, 15.879175° S 65.858939° W. See Supplemental Figure 2 for Landsat image progression of this process.

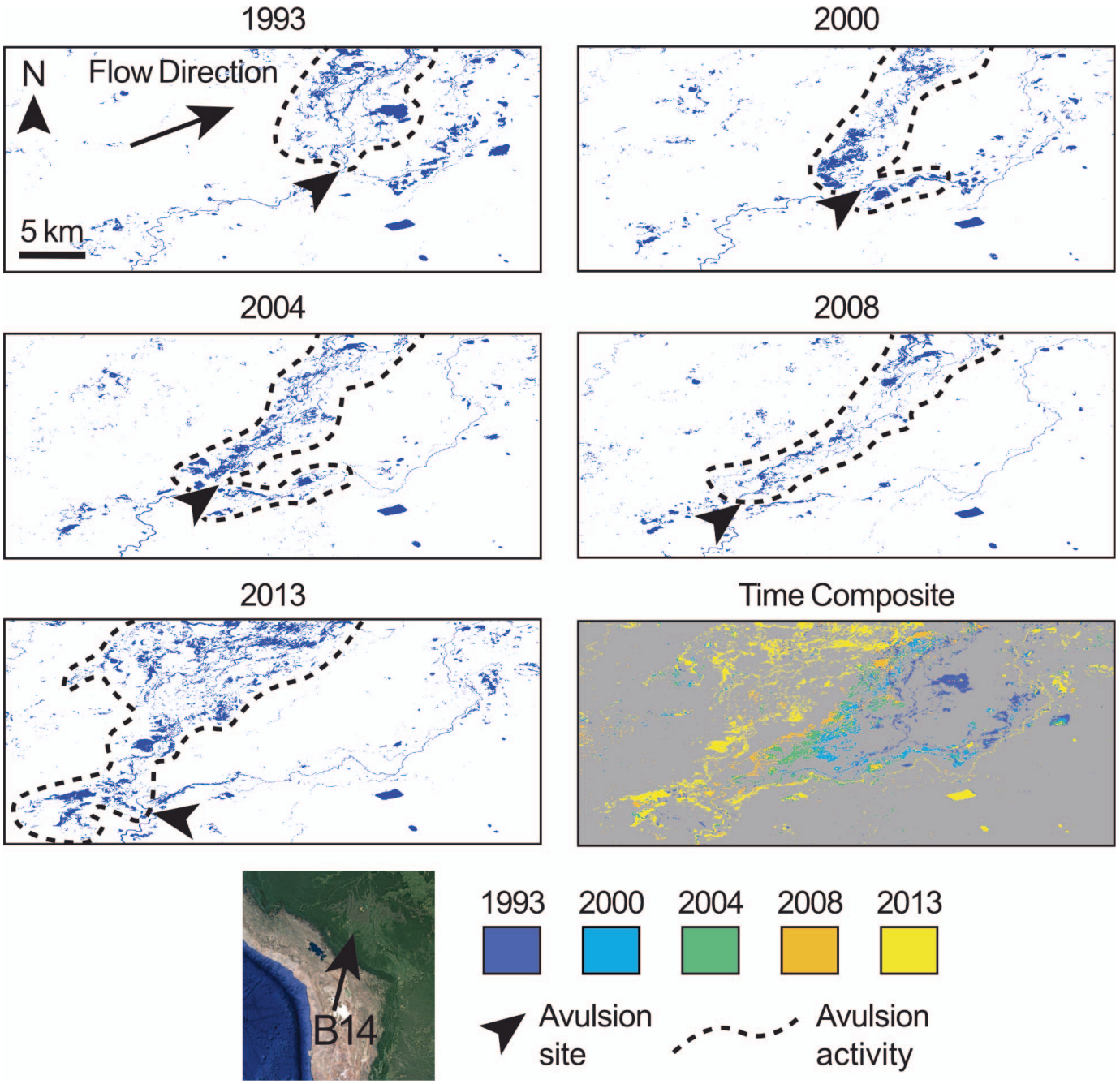

FIG. 9.—Retrogradation is accompanied by significant overbank activity over time. The time composite panel shows all years in a flattened image. Note that the point of diversion continues to migrate upstream each year. Progradational processes such as distributary-network formation and nonchannelized flow are seen in progressively upstream locations as well, marked by a dashed line. Avulsion sample B14, 14.677489° S 66.530844° W.

that this process continues until the dechannelized flow is redirected into a relict or local channel, or when it develops into a distributary network that coalesces into a new channel capable of transporting diverted flow. For more information about the conditions that foster retrogradational avulsions see Lombardo (2017) and Edmonds et al. (2022).

How Do the Various Avulsion Processes Interact?

Avulsion fingerprinting reveals an often-pronounced alternation between the various avulsion processes through space and time. For example, avulsion B9 on the Moleto River, Bolivia, demonstrates how all three processes contribute to a single avulsion event (Fig. 10). This avulsion began when the parent channel migrated laterally into a small headward-eroding local channel that captured flow from the Moleto River parent channel. Over the span of a year the flow from the parent channel was rapidly diverted into the annexed channel. In response to the sudden increase in discharge, the annexed channel increased its width, and the meander wavelength and amplitude were rapidly overprinted through cutoffs and channel migration (Fig. 10A). Thirty-five kilometers downstream of this annexational reach, the avulsion regime changed to

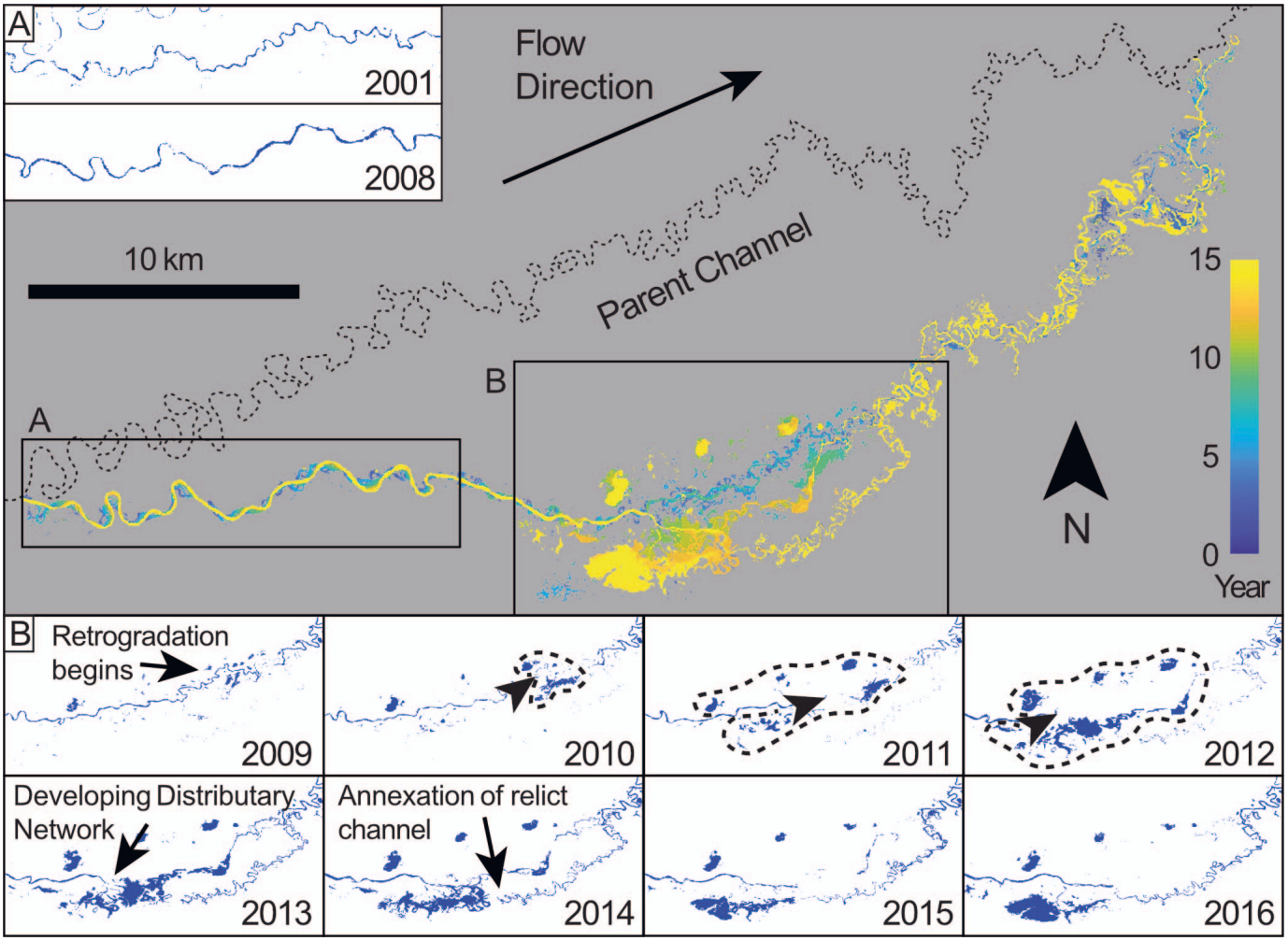

FIG. 10.—Sample B9 (Rio Moleto, Bolivia) demonstrates annexational, progradational, and retrogradational processes. **A)** The initial avulsion reach shows annexation, with no floodplain disturbance, and from year 2001 to 2008 the channel width and meander wavelength and amplitude increased to accommodate parent-channel discharge. **B)** At a downstream location, retrogradation begins in 2009, and moves upstream 10 km by 2012 (activity is marked by dashed line, arrowheads in 2010–2012 mark the upstream-migrating avulsion site). In 2013, progradation begins and a distributary network developed. In 2016 a northern branch of the distributary network became the primary channel, and quickly annexed another local channel which connected back to the first annexed channel. Avulsion B9 initiates at 16.321883° S 65.840436° W.

retrogradation in 2009. During retrogradation, flooding on either side of the channel migrated upstream for ~10 kilometers until 2013 (Fig. 10B). At this point, a large splay on the south side of the original avulsion channel prograded downstream until it annexed another local channel (Fig. 10B, year 2016). This final phase reconnected the retrograded and prograded reaches with the originally annexed channel path approximately 40 kilometers downstream from the initial avulsion site (Fig. 10B).

Avulsion B1, on the Grande River, Bolivia, offers another example of how avulsion processes interact. The first reach of the event, from the initial avulsion site to roughly 90 kilometers downstream, demonstrated short-lived, nonchannelized flow tens of kilometers beyond parent and avulsion channels. Downstream from this reach, most of the avulsion activity was dominated by the filling in of pre-existing and newly created lakes (Fig. 11A). These lakes were separated by 1–20 km zones of channel annexation. Looking closer at this "chain of lakes" reach, from 1994 to 2015 pre-existing and newly created lakes were filled as avulsion activity evolved in that reach. Beyond this initial lake-filling reach, the avulsion annexed a channel and was accompanied by a few small clusters of unidentified floodplain activity. For the final 50 km of this avulsion, we observe the recurrence of the chain-of-lakes behavior. However, rather than causing significant infilling as in the first chain-of-lake reach, only one lake disappeared completely, and the rest experienced varying degrees of modification by the avulsed flow.

Recognizing that stratigraphic temporal resolution is typically coarser than the annual resolution provided by our dataset, we first focus on quantifying the spatial variability of avulsion activity. To this end, we plot S_{RN} as a function of distance downstream along the final avulsion channel-belt centerline, (Figs. 3, 12). Considering activity in this way does not allow differentiation between progradational and retrogradational activity, but it does highlight reaches where activity remained restricted to channels (low S_{RN}) or spread across the floodplain (high S_{RN}). Eleven of 13 events either begin or end with reaches of $S_{RN} < 3$, and 7 of 13 both begin and end with $S_{RN} < 3$ (Fig. 12). The fact that so many initial and terminal reaches demonstrate exclusively annexational activity highlights the fundamental importance of annexation to avulsion initiation and resolution. Exceptions to annexation in initial and terminal reaches include avulsions B10, G1, and V7, which start with high S_{RN} values but decrease with distance, and avulsion V11, which begins with low S_{RN}, increases with distance, and maintains high S_{RN} along the rest of the avulsion belt. In middle reaches, avulsions often have one or more progradational or

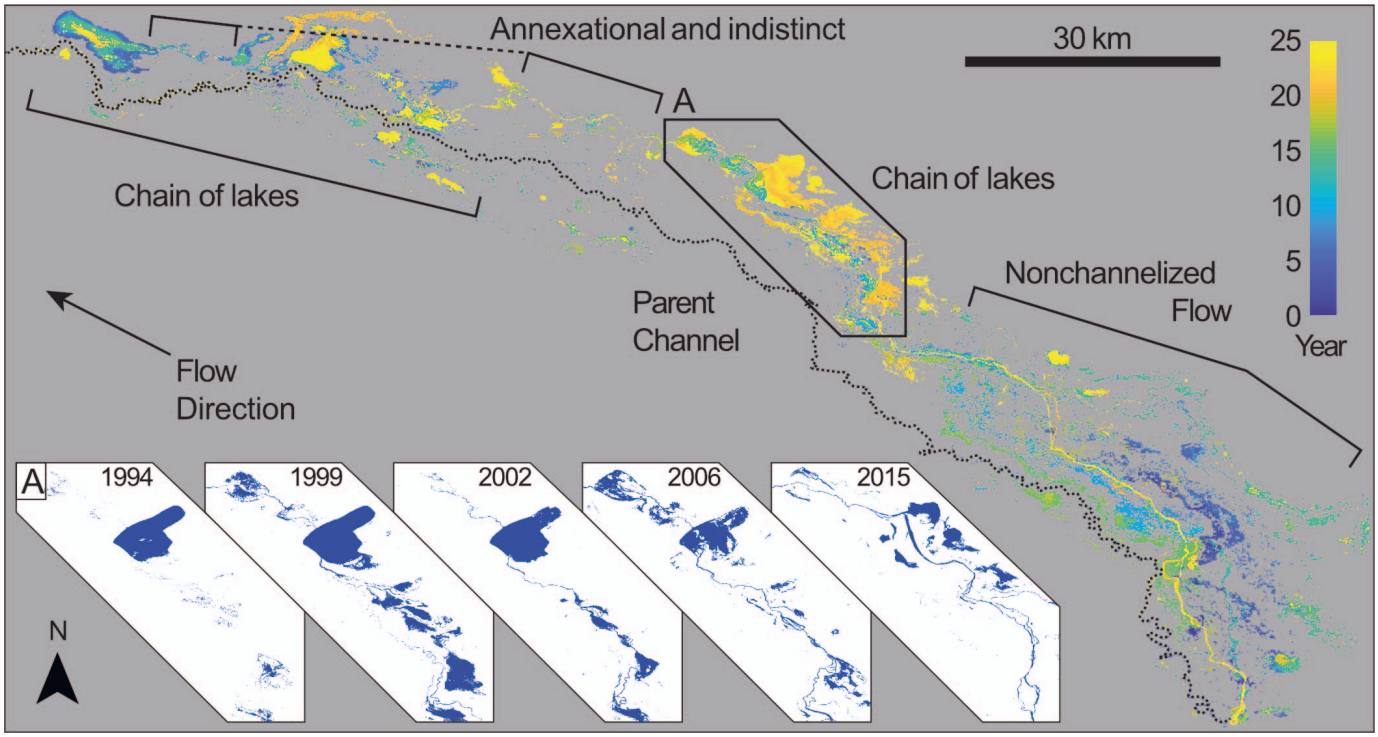

FIG. 11.—Sample B1, located on the Grande River, Bolivia. This avulsion demonstrates annexation and progradation. The latter two-thirds of the avulsion is dominated by a series of ponds connected by channels. **A)** Creation and infilling of ponds by avulsion activity. Avulsion B1 initiates at 17.036376° S 62.984473° W.

retrogradational sub-reaches. Fluctuations in S_{RN} in every avulsion in Figure 12 underscores the inherent non-uniformity of avulsion activity along a given avulsion belt. This also suggests that progradation tends to occur on the floodplain away from the parent channel and relict or local channels. Sample B14 shows yet another mode, where several exceptionally high peaks are isolated by mostly low S_{RN} values, representing large, isolated progradational reaches.

Among the larger dataset of Valenza et al. (2020), annexation is by far the most commonly observed process. While 50 of 63 avulsions proceeded exclusively through annexation, 12 of the remaining 13 avulsions classified as predominantly progradational ($S_R > 2$) by Valenza et al. (2020) host annexational reaches, as defined by the presence of nodes with $S_{RN} < 3$ (Table 1). More specifically, annexational reaches constitute up to 60% of avulsion-belt lengths, with an average of 22.4%. Eleven of 13 events either begin or end with annexation, and seven both begin and end with annexation. Thus, annexation appears to be the default avulsion process, giving way to progradation or retrogradation when: 1) there are no suitable relict or local channels nearby or 2) an annexed channel cannot contain the diverted discharge from the parent channel. Conversely, prograding or retrograding reaches revert to annexation upon encountering a channel capable of transporting the new discharge.

How Do Avulsion Belts Progress Across the Floodplain?

A new avulsion pathway is created by annexation, progradation, and/or retrogradation. These processes influence how the avulsion belt progresses across the floodplain through time and space. We quantify the spatiotemporal progression of the avulsion belt by plotting the center of avulsion activity each year (Fig. 13). Some avulsions demonstrate a predominantly downstream migration of center of avulsion activity, indicating that progradation is a dominant process in those events (B12, G5, G12, V7, V11, V14). Other events demonstrate significant upstream migration of activity, highlighting the importance of retrogradation to those events (B1, B9, B14, G2). Upstream-migrating activity follows one of two patterns, the first of which includes a sudden backstepping (B12, G1, G2, G12, V11), where activity jumps several nodes upstream in one year. This pattern suggests the avulsion pathway was primed for avulsion at multiple locations, and a new event was triggered upstream from an earlier avulsion site (either randomly or due to a backwater effect). The second retrogradational pattern displays multi-year episodes of gradual upstream migration (B1, B9, B10, B12, B14, G8, G12, V7, V14), suggesting an upstream-migrating feedback cycle (Edmonds et al. 2022). The rest of the events exhibit relatively stationary (B10, G1, G8, H5) centers of avulsion activity, suggesting that diverted water and sediment are mostly constrained to one area, possibly due to high accommodation, or that discharge remains low enough as to prevent observable changes. In all three groups, variability is superimposed on general trends. This underscores that no avulsion in this study progresses monotonically upstream or downstream, but rather experiences distinct, often alternating phases of annexation, progradation and/or retrogradation.

DISCUSSION

Implications for Building Floodplains and Avulsion Stratigraphy

Our avulsion fingerprinting method is tuned to find pixels that experience flooding, sedimentation, or vegetation reduction, all of which are primary indicators of avulsion-related activity. Mapping this activity through space and time allows us to examine and characterize how avulsions progress across their floodplains, as well as predict potential locations and modes of sediment deposition and floodplain channel reworking.

The fact that we observe various combinations of annexation, progradation, and retrogradation confirms the idea that floodplain environments are composed of a patchwork of localized hydrological environments (Trigg et al. 2012; Davidson et al. 2013; Hajek and Edmonds

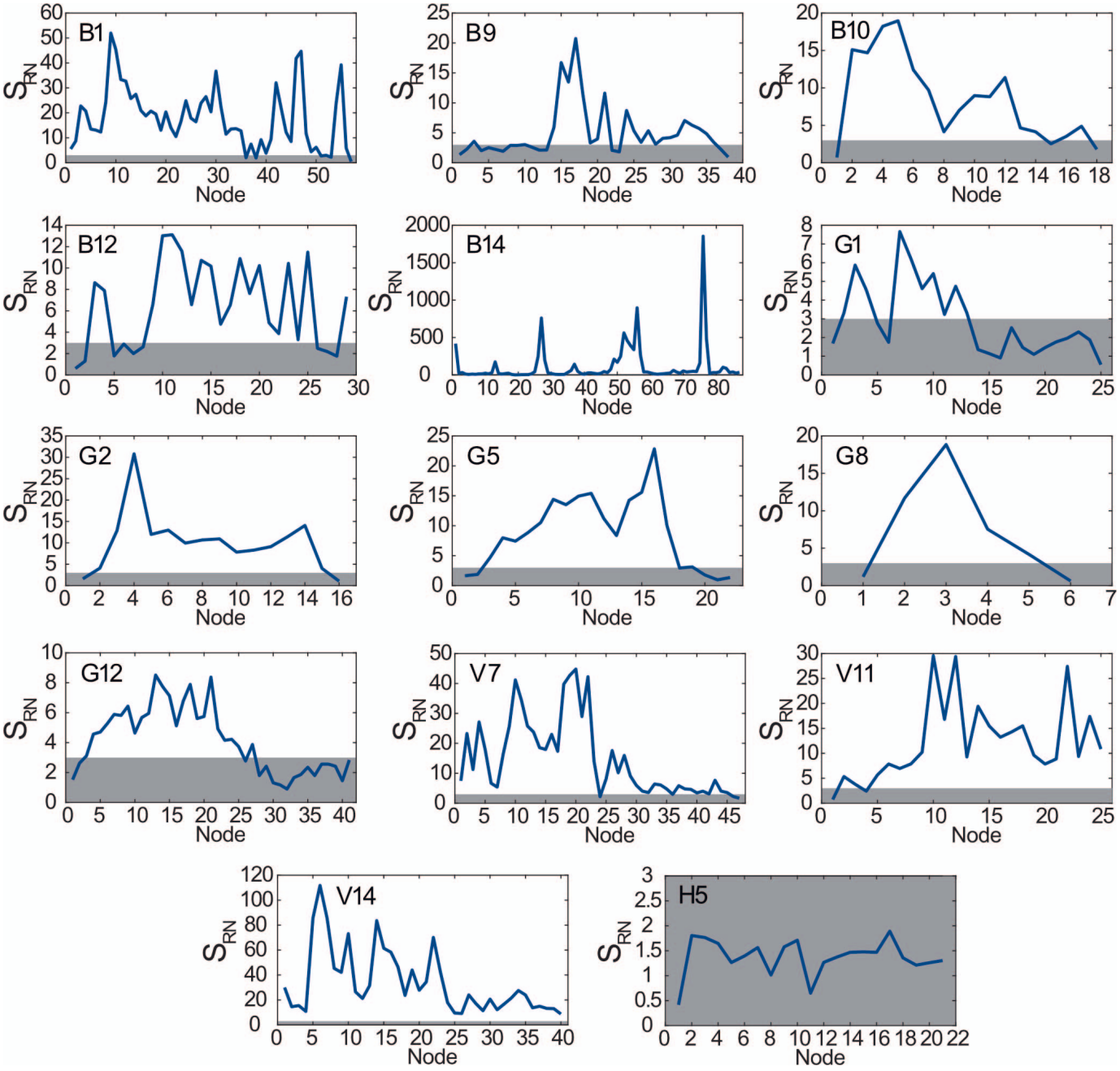

FIG. 12.—Nodal avulsion style ratio (S_{RN}) as a function of distance along each avulsion belt. Nodes are numbered from upstream to downstream and are spaced at intervals of ten times the channel width (except avulsions G5, G12, and H5, which were measured at intervals equal to the corresponding parent width) along avulsion channel centerline. Blue curves represent S_{RN}. Grayed area is $S_{RN} < 3$, which we interpret as annexational activity. Note that S_{RN} does not distinguish between progradational and retrogradational activity.

2014; Edmonds et al. 2016). These range from well-drained and channelized to poorly drained, marshy, and sparsely channelized (Aslan and Autin 1999; Morozova and Smith 2000; Fagan and Nanson 2004; Day et al. 2008; David et al. 2017). In some locations, the floodplain may be dominated by large swaths of similar hydrological environments, such as proximal fan settings which host densely packed relict channel belts (Weissmann et al. 2010; Davidson et al. 2013). However, except for sample V14, even predominantly poorly drained hydrological environments host some locally well-drained sub-environments, which causes avulsion activity to shift back and forth between different processes.

Avulsion stratigraphy is generally described by end-member styles resulting from progradational avulsions (Smith et al. 1989; Smith and Perez-Arlucea 1994; Perez-Arlucea and Smith 1999; Slingerland and Smith 2004; Assine 2005; Buehler et al. 2011; Louzada et al. 2020) or annexational avulsions (Jones and Harper 1998; Field 2001; Makaske et al. 2002; Jones and Hajek 2007; Chakraborty and Ghosh 2010). These previous studies show that progradation produces heterolithic facies packages (Kraus et al. 1999; Jones and Hajek 2007) consisting of overbank deposition including crevasse splays and deltas (Smith et al. 1989; Smith and Perez-Arlucea 1994; Perez-Arlucea and Smith 1999; Morozova and

TABLE 1.—*Avulsion event node counts, number of annexational nodes, percentage of nodes that are annexational, avulsion-belt length, parent-channel width, normalized distance from the mountain front, and lat./long. coordinates. Normalized distance refers to the length of the parent-channel belt from the mountain front to the initiation site, divided by the parent-channel width at that site (Valenza et al. 2020).*

Avulsion Events	Total Nodes	Annex. Nodes	% Annex.	Avulsion-Belt Length (km)	Parent-Channel Width (m)	Normalized Distance from Front	Lat.	Long.
B1	57	6	10.5	198	400	622.5	–17.0815	–62.9795
B9	38	15	39.5	60.5	159	382.4	–16.3225	–65.8384
B10	18	3	16.7	85.8	164	505.5	–16.2728	–65.2038
B12	29	9	31	48.4	98	505.1	–15.879	–65.859
B14	87	2	2.3	78.3	110	1218.2	–14.677	–66.5308
G1	25	15	60	36.1	154	386.4	–5.726	145.527
G2	16	2	12.5	5.4	38	215.4	–5.1578	144.7887
G5	22	6	27.3	9.3	360	23.9	–4.1512	135.244
G8	6	2	33.3	5.8	82	270.2	–3.9686	135.0749
G12	41	17	41.5	6.5	148	27	–6.6624	147.0569
V7	47	4	8.5	17.1	57	1226.3	6.73	–71.2565
V11	25	2	8	24.3	110	749.1	7.1703	–71.345
V14	40	0	0	34	90	774.4	8.4146	–69.9831
H5	21	21	100	33.9	1500	0.3	26.7836	90.9566

Smith 2000; Slingerland and Smith 2004). In contrast, annexation does not produce as much deposition, and creates new channel-sand bodies and/or multi-story sand bodies with saw-tooth edges (e.g., Chamberlin and Hajek 2015).

During progradation we see crevasse-splay advancement (Fig. 6) and delta deposition in standing water (Figs. 7, 11), along with nonchannelized activity (Figs. 8, 9). We expect these processes to create the heterolithic packages observed in the stratigraphic record. Additionally, the strong tendency towards annexation observed in our data suggests that multi-story sand bodies are potentially the most common indicator of avulsion in the stratigraphic record. This is consistent with Chamberlain and Hajek (2015), who found that the most unambiguous indicator of avulsion is multi-storied channel bodies with saw-toothed margins. The saw-toothed margins are a clear indication of abandonment and reoccupation (i.e., annexation). We note, however, that story boundaries can result from a variety of other channel processes unrelated to avulsion. These include seasonal discharge fluctuation (Tunbridge 1981; Olsen 1989), meander cutoff (Platt and Keller 1992; Corbett et al. 2011), channel-thread migration (Johnson and Pierce

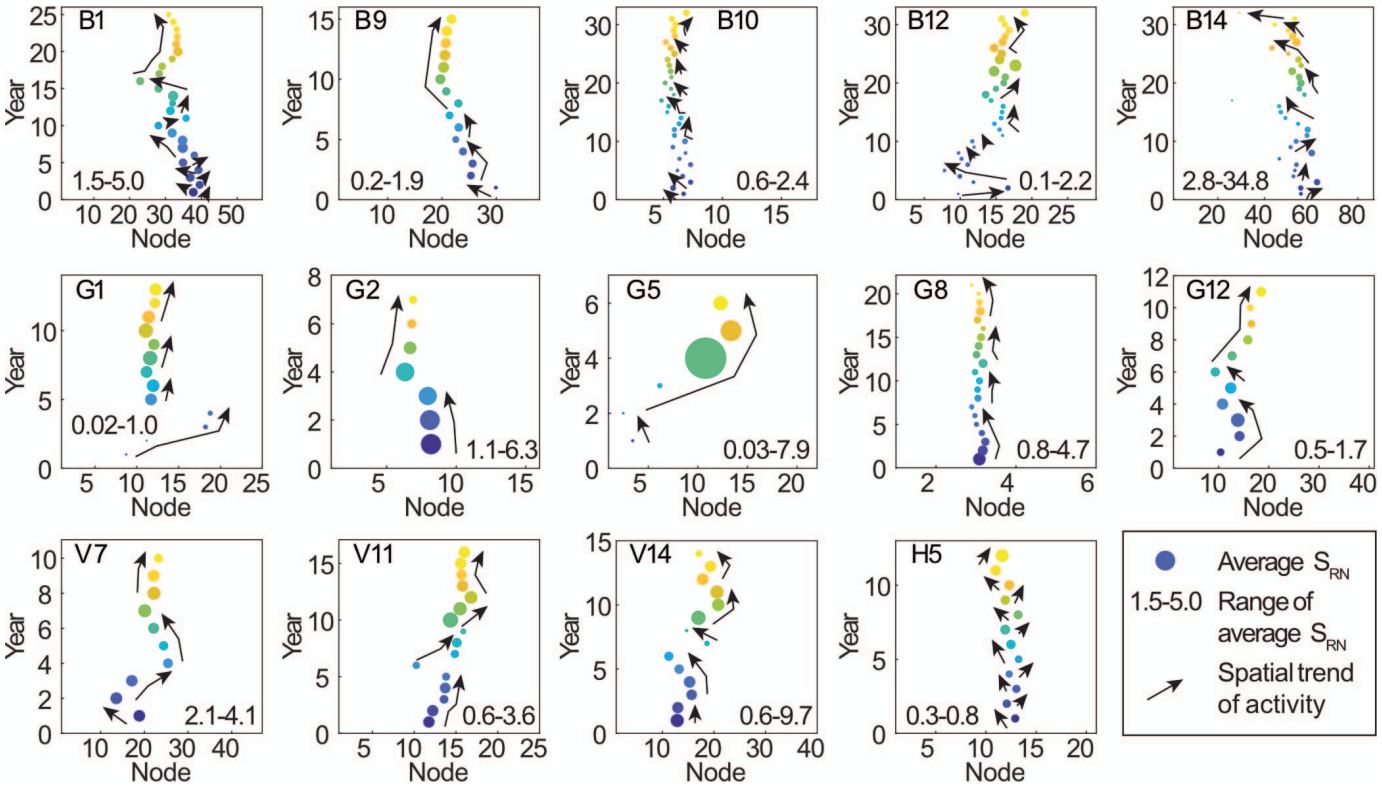

FIG. 13.—Spatiotemporal progression of each avulsion belt. We calculate the center of mass of all avulsion pixels for each year. The size of the points is proportional to the mean S_{RN} for that year, and maximum and minimum values of the averaged S_{RN} in the lower part of each plot are provided for scale. The point color corresponds to year, with cool colors representing earlier years and warm colors later years. The absolute years vary from plot to plot.

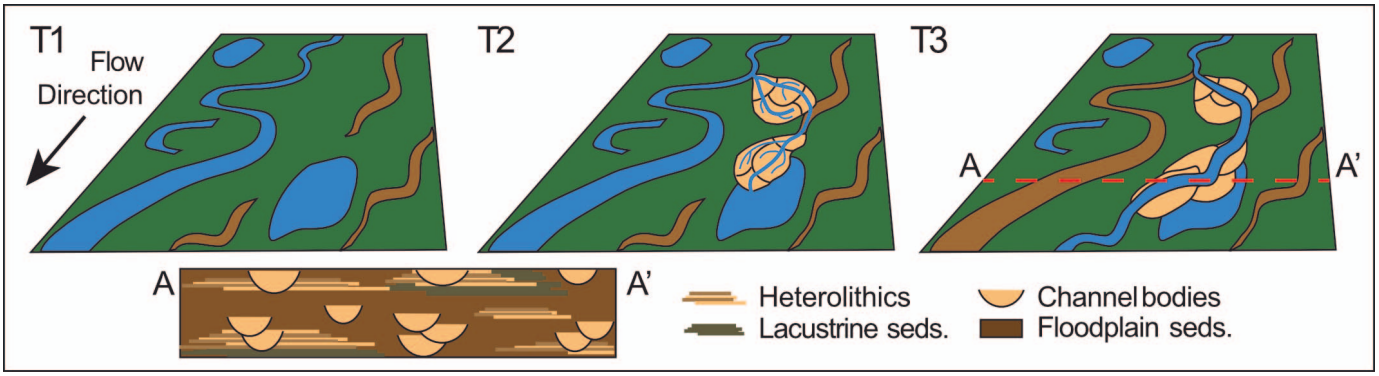

FIG. 14.—Conceptual model of a hybrid-style avulsion. In T1, a heterogeneous floodplain is marked by relict and local drainage channels, oxbow lakes, and floodplain ponds. In T2, the parent channel has migrated into a relict channel, triggering annexation as flow is diverted. As the annexed channel narrowed, flow was forced onto the floodplain as a distributary network, which continued to prograde into a pond. By T3, the prograding distributary network has filled much of the pond, proceeded past it onto the floodplain into a local drainage channel, and has coalesced into a new primary channel. Cross section from A–A′ shows the expected mix of stratigraphic features, including single-story or multi-story channel bodies, in some cases isolated in floodplain fine-grained sediments, and in others incising into overbank heterolithics from progradational and retrogradational deposits. Modified from Mohrig et al. (2000).

1990), and bar migration (Diemer and Belt 1991; Kumar 1993; Labourdette and Jones 2007).

Our results provide two additional perspectives on avulsion style and the associated deposits that avulsion facies models do not currently capture (e.g., Smith et al. 1989; Kraus et al. 1999; Mohrig et al. 2000; Slingerland and Smith 2004). The first is that "progradational avulsions" typically host a combination of progradational, retrogradational, and annexational reaches (Figs. 12, 13). Consequently, we expect that these events produce diverse stratigraphic components, making it challenging to define an avulsion simply as progradational or annexational in the stratigraphic record. Thus, non-annexational avulsions are probably best characterized by a hybrid facies model that includes both progradation (or retrogradation) and annexation (Fig. 14). This hybrid model suggests that any one outcrop could demonstrate a variety of facies related to progradation, retrogradation, and annexation. Considering that on average 22.4% of the avulsion-belt lengths were annexational (Table 1), and avulsion-belt lengths and widths ranged from 5 to 60 km and from 1 to 50 km respectively, annexational architecture could comprise as little as several hundred meters to more than 10 km of the length or width of an otherwise progradational stratigraphic package. Consequently, it is probably impossible to fully characterize the style of any one avulsion belt, especially with limited longitudinal exposure. Avulsion stratigraphy is then best characterized by considering the range of avulsion deposits at the outcrop or member scale. For example, by looking at the avulsion facies of all channel belts in a single member, one could determine the proportion of channels that are annexational (or progradational). This would provide a time-averaged sense of the dominant avulsion style at that location (e.g., Hajek and Edmonds 2014). Interesting and unexplored possibilities emerge if these data are collected over space. As Valenza et al. (2020) showed in modern foreland basins, avulsion events become more progradational in the downstream direction. This trend could be tested in ancient systems by determining how the proportion of annexational channels to progradational packages in a stratigraphic succession changes along the sediment route. Changing proportions of avulsion products downstream may be an unappreciated control on fluvial stacking patterns and stratigraphic architecture, and, for instance, may influence the proximal–distal patterns identified by Weissmann et al. (2013) in megafans.

A second addition to current avulsion facies models includes the products of retrogradation (Edmonds et al. 2022). Retrogradational deposits, at a given location, should differ from progradation because of the sense of movement of the sediment source. Our data and those from Edmonds et al. (2022) show that retrogradational avulsion nodes migrate upstream. This upstream migration could create a fining-upward grain-size trend for the avulsion deposits. The initial deposits would be coarse given the proximity to the front of the upstream-migrating wave of sedimentation. Once the front moves upstream and becomes more distant, the sediment should fine. This is the opposite of prograding distributary networks, which create coarsening-upward successions as they prograde over previously deposited material that, at the time, was relatively distal to the avulsion initiation site. This simple hypothesis could be tested by coring the locations where avulsions in this study experienced retrogradation.

Avulsion Pathfinding

Previous work (Valenza et al. 2020) suggests that annexation is the most commonly occurring avulsion process, and our data indicate that annexation plays a significant role in even largely progradational events. It then follows that the most important determinant of avulsion process is the arrangement, density, and character of annexable channels on the floodplain. While several studies mapped relict and active channels on megafans (Chakraborty et al. 2010; Chakraborty and Ghosh 2010; Zani et al. 2012; Zani and De Fátima Rossetti 2012), channel density on fans or floodplains has rarely been examined systematically. Recent studies suggest that inactive channels are surprisingly common on some meandering-river floodplains (David et al. 2017; Czuba et al. 2019). Lidar data from meandering-river floodplains in Indiana, USA, reveals that almost 40% of studied floodplains were densely populated with relict channels that could facilitate avulsion by annexation. Indiana is not in a tectonically active, aggradational environment, and lidar surveys in active foreland basins are needed to measure floodplain channel density and characteristics, providing a means to test the idea that greater channel density results in more annexation. By contrast, progradation or retrogradation may dominate when floodplain channel density is low. Thus, the prevalence of the various avulsion processes may be related to the character and density of relict or local channels on a given floodplain. Furthermore, the processes involved in retrofitting an annexed channel are also important, including the rate of channel widening and/or changing meander wavelength and amplitude (Figs. 4, 10A). For example, when retrofitting occurs too slowly, the annexation of the channel fails and results in progradation or retrogradation.

Finally, our data suggest that annexation serves as the dominant style at the beginning and end of the avulsion pathway (Fig. 12). This, in turn, suggests that annexation is an important process for initiating and

resolving avulsions. However, most avulsion initiation models rely on superelevation to predict when and where avulsions occur (Slingerland and Smith 1998; Jones and Schumm 1999; Mohrig et al. 2000; Törnqvist and Bridge 2002; Jerolmack and Mohrig 2007; Jobe et al. 2020). Superelevation occurs when sediment aggradation on the channel bed raises, or superelevates, the bed with respect to the average floodplain elevation. As superelevation increases, avulsion becomes more likely as flow paths beyond the parent channel become more efficient than the active flow path (Brizga and Finlayson 1990; Slingerland and Smith 1998; Mohrig et al. 2000; Törnqvist and Bridge 2002). When an avulsion occurs in this state there should be significant deposition as the bed load is redirected onto the floodplain. Most superelevation criteria do not account for the presence of relict or local floodplain channels, and our data suggest that the presence of such floodplain channels close to the primary channel may be an overlooked contributor to the cause of river avulsions.

Limitations of Our Analyses

Our analyses carry several notable limitations. First, the data we present come from self-formed river systems draining active orogenic belts. These events occur primarily in medial to distal positions in alluvial fan or megafan floodplains (e.g., distributive fluvial systems of Weissmann et al. (2010)), except for sample H5, which occurs in a proximal fan position and is exclusively annexational. All events occur on floodplains unrestricted by either bedrock or alluvium-terraced river valleys.

A second limitation is that we do not have field measurements of land-surface change to confirm our remote-sensing analyses. For instance, we assume that annexation occurs when $S_{RN} < 3$, and in some cases, we directly observed avulsions annexing relict or local channels (Figs. 4, 5). In other cases, we could not identify obvious preexisting channels, in which we suggest that values of $S_{RN} < 3$ may be due to incision, non-deposition, or poor data resolution (Fig. 12). In the case of poor spatial resolution, preexisting channels may not be resolvable because they are filled with vegetation, covered by forest canopy, or have widths below 30-m Landsat pixel resolution. In the case of poor temporal resolution, discharge may have in fact left the parent channel, but floodplain disturbance was so short lived as to have initiated and resolved between available Landsat data. We consider these approximations acceptable because in both cases, discharge is so low that it leaves floodplain surfaces undisturbed by scouring, drowning, or sediment burial. If diverted flow is reaching floodplain locations but not causing any lasting disturbances, then it is not likely depositing significant volumes of sediment or significantly modifying the floodplain surface.

A third limitation is that our data do not distinguish between incision and annexation. While some authors suggest that incisional avulsions constitute a distinct style (Slingerland and Smith 2004; Jones and Hajek 2007), we consider them a type of annexation, given that they result in little to no floodplain disturbance and could be difficult to distinguish from annexational events in the rock record. Distinguishing between annexation and incision with Landsat imagery is challenging because not every incipient avulsion channel is clearly visible before annexation (potentially due to a sub-pixel scale or vegetation cover). We interpret all avulsions that maintain observable channelization from the initiation site and time of avulsion through the establishment of a new channel path to represent annexational behavior. Overland flow that incises a new channel into previously nonchannelized floodplain would map as widespread flooding, or nonchannelized flow, before channelization and appear as progradational overbank activity. Without ground-truthing to establish the degree of sedimentation or scouring, we are left to interpret the transition of nonchannelized flow to channelized flow as a progradational process.

Finally, we acknowledge that using modern sedimentary systems to understand ancient environments is not always straightforward. For example, extreme climate cycling during the Pleistocene and Holocene likely introduces greater variability than is common throughout geologic time (Poore et al. 2003; Mayewski et al. 2004). This variability may cause more frequent avulsion triggers compared to other climatic forcings (Morón et al. 2017).

CONCLUSIONS

Using Landsat data, we characterized the avulsion activity of 13 events that occurred in Andean, Himalayan, and New Guinean foreland basins (plus H5 for comparison). We selected these events because they exhibit significant progradation, yet for all but one event we found that avulsion proceeded through some combination of annexation, progradation, and retrogradation. Annexation is marked by reoccupation and subsequent channel adjustments, including widening, increasing meander wavelength and amplitude, and/or an increase in the number of channel threads. Progradation is marked by channel construction and a range of floodplain activity, both resulting from crevassing, evolution of distributary networks, creation and filling of ponds, and nonchannelized flow. Retrogradation is marked by a persistent upstream migration of channel extinction flanked by short-lived overbank flow.

Notably, we found that annexation played a significant role in all but one avulsion event. On average 22.4% of avulsion-belt lengths were annexational, with sample G1 exhibiting annexation over 60% of its length. Furthermore, 11 avulsions hosted annexational reaches at the beginning or end of their avulsion belts, and seven avulsions hosted annexation at both the beginning and end of their belts, indicating the importance of this process to avulsion initiation and resolution. Furthermore, this suggests that even progradational avulsions are hybrid events that contain more than one avulsion process. Because avulsion-belt lengths and widths ranged from 5 to 60 km and from 1 to 50 km, respectively, resulting annexational architecture could comprise as little as several hundred meters to more than 10 km of the length or width of an otherwise progradational and/or retrogradational stratigraphic package. This variability is also reflected in how avulsions move across the floodplain. Avulsions can move downstream (through progradation), upstream (through retrogradation), or remain stationary (through annexation), and most events display some combination of these movements through time.

Traditionally, avulsions have been categorized broadly as either annexational or progradational. Our data suggest that annexation, progradation, and retrogradation often occur in the same event. Annexation serves as the default avulsion process, and if the annexed channel can accommodate all diverted flow, the avulsion occurs quickly and without further activity beyond channel adjustment to new discharge. In cases where no channel is available for annexation, or an annexed channel cannot accommodate the new discharge, flow is diverted onto the floodplain, resulting in either progradation or retrogradation. The stratigraphic record of a single avulsion event may include the sedimentary products of all these processes, including stacked channel bodies from annexation, a variety of heterolithic overbank packages from progradation, and fining-upward successions from retrogradation. These hybrid events likely produce significantly greater stratigraphic variability than that predicted by the traditional end-member model. Thus, accurate interpretation of ancient fluvial systems requires a time-averaged, formation-scale consideration of avulsion strata.

SUPPLEMENTAL MATERIAL

Supplemental material is available from the SEPM Data Archive: https://www.sepm.org/supplemental-materials.

ACKNOWLEDGEMENTS

JMV and DAE were supported by National Science Foundation grant 1911321. All data and code from this paper is available at IUScholarWorks at https://hdl.handle.net/2022/27050.

REFERENCES

Allen, J.R., 1965, A review of the origin and characteristics of recent alluvial sediments: Sedimentology, v. 5, p. 89–191.

Aslan, A., and Autin, W.J., 1999, Evolution of the Holocene Mississippi River floodplain, Ferriday, Louisiana: insights on the origin of fine-grained floodplains: Journal of Sedimentary Research, v. 69, p. 800–815.

Assine, M.L., 2005, River avulsions on the Taquari megafan, Pantanal wetland, Brazil: Geomorphology, v. 70, p. 357–371.

Baig, M.H.A., Zhang, L., Shuai, T., and Tong, Q., 2014, Derivation of a Tasselled Cap Transformation based on Landsat 8 at-satellite reflectance: Remote Sensing Letters, v. 5, p. 423–431.

Bridge, J.S., and Leeder, M.R., 1979, A simulation model of alluvial stratigraphy: Sedimentology, v. 26, p. 617–644.

Bridge, J., and Mackey, S., 1993, A revised alluvial stratigraphy model, *in* Marzo, M., and Puigdefabregas, C., eds., Alluvial Sedimentation: Hoboken, Wiley-Blackwell, p. 317–336.

Brierley, G.J., Ferguson, R.J., and Woolfe, K.J., 1997, What is a fluvial levee?: Sedimentary Geology, v. 114, p. 1–9.

Bristow, C.S., 1987, Brahmaputra River: channel migration and deposition, *in* Ethridge, F.G., Flores, R.M., and Harvey, M.D., eds., Recent Developments in Fluvial Sedimentology: SEPM, Special Publication 39, p. 63–74.

Brizga, S.O., and Finlayson, B.L., 1990, Channel avulsion and river metamorphosis: the case of the Thomson River, Victoria, Australia: Earth Surface Processes and Landforms, v. 15, p. 391–404.

Buehler, H.A., Weissmann, G.S., Scuderi, L.A., and Hartley, A.J., 2011, Spatial and temporal evolution of an avulsion on the Taquari River distributive fluvial system from satellite image analysis: Journal of Sedimentary Research, v. 81, p. 630–640.

Burns, C.E., Mountney, N., Hodgson, D., and Colombera, L., 2017, Anatomy and dimensions of fluvial crevasse-splay deposits: examples from the Cretaceous Castlegate Sandstone and Neslen Formation, Utah, USA: Sedimentary Geology, v. 351, p. 21–35.

Chakraborty, T., and Ghosh, P., 2010, The geomorphology and sedimentology of the Tista megafan, Darjeeling Himalaya: implications for megafan building processes: Geomorphology, v. 115, p. 252–266.

Chakraborty, T., Kar, R., Ghosh, P., and Basu, S., 2010, Kosi megafan: historical records, geomorphology and the recent avulsion of the Kosi River: Quaternary International, v. 227, p. 143–160.

Chamberlin, E.P., and Hajek, E.A., 2015, Interpreting paleo-avulsion dynamics from multistory sand bodies: Journal of Sedimentary Research, v. 85, p. 82–94.

Corbett, M.J., Fielding, C.R., and Birgenheier, L.P., 2011, Stratigraphy of a Cretaceous coastal-plain fluvial succession: the Campanian Masuk Formation, Henry Mountains syncline, Utah, USA: Journal of Sedimentary Research, v. 81, p. 80–96.

Crist, E.P., 1985, A TM tasseled cap equivalent transformation for reflectance factor data: Remote Sensing of Environment, v. 17, p. 301–306.

Crist, E.P., and Cicone, R.C., 1984, A physically-based transformation of Thematic Mapper data: the TM Tasseled Cap: Institute of Electrical and Electronics Engineers, Transactions on Geoscience Remote Sensing, p. 256–263.

Crist, E.P., and Kauth, R., 1986, The Tasseled Cap de-mystified: Photogrammetric Engineering and Remote Sensing, v. 52, p. 81–86.

Czuba, J.A., David, S.R., Edmonds, D.A., and Ward, A.S., 2019, Dynamics of surface-water connectivity in a low-gradient meandering river floodplain: Water Resources Research, v. 55, p. 1849–1870.

David, S.R., Edmonds, D.A., and Letsinger, S.L., 2017, Controls on the occurrence and prevalence of floodplain channels in meandering rivers: Earth Surface Processes and Landforms, v. 42, p. 460–472.

Davidson, S.K., Hartley, A.J., Weissmann, G.S., Nichols, G.J., and Scuderi, L.A., 2013, Geomorphic elements on modern distributive fluvial systems: Geomorphology, v. 180, p. 82–95.

Day, G., Dietrich, W.E., Rowland, J.C., and Marshall, A., 2008, The depositional web on the floodplain of the Fly River, Papua New Guinea: Journal of Geophysical Research: Earth Surface, v. 113, no. F01S02.

Diemer, J.A., and Belt, E.S., 1991, Sedimentology and paleohydraulics of the meandering river systems of the Fort Union Formation, southeastern Montana: Sedimentary Geology, v. 75, p. 85–108.

Donselaar, M., Gozalo, M.C., and Moyano, S., 2013, Avulsion processes at the terminus of low-gradient semi-arid fluvial systems: lessons from the Río Colorado, Altiplano endorheic basin, Bolivia: Sedimentary Geology, v. 283, p. 1–14.

Edmonds, D.A., Hajek, E.A., Downton, N., and Bryk, A.B., 2016, Avulsion flow-path selection on rivers in foreland basins: Geology, v. 44, p. 695–698.

Edmonds, D.A., Martin, H.K., Valenza, J.M., Henson, R., Weissmann, G.S., Miltenberger, K., Mans, W., Moore, J.R., Slingerland, R.L., and Gibling, M.R., 2022, Rivers in reverse: upstream-migrating dechannelization and flooding cause avulsions on fluvial fans: Geology, v. 50, p. 37–41.

Ethridge, F., Skelly, R., and Bristow, C., 1999, Avulsion and crevassing in the sandy, braided Niobrara River: complex response to base-level rise and aggradation, *in* Smith, N.D., and Rogers, J., eds., Fluvial Sedimentology VI: International Association of Sedimentologists, Special Publication 28, p. 179–191.

Fagan, S.D., and Nanson, G.C., 2004, The morphology and formation of floodplain-surface channels, Cooper Creek, Australia: Geomorphology, v. 60, p. 107–126.

Field, J., 2001, Channel avulsion on alluvial fans in southern Arizona: Geomorphology, v. 37, p. 93–104.

Flood, Y.S., and Hampson, G.J., 2014, Facies and architectural analysis to interpret avulsion style and variability: Upper Cretaceous Blackhawk Formation, Wasatch Plateau, Central Utah, USA: Journal of Sedimentary Research, v. 84, p. 743–762.

Gole, C.V., and Chitale, S.V., 1966, Inland delta building activity of Kosi River: American Society of Civil Engineers, Proceedings, Journal of the Hydraulics Division, v. 92, is. 2, p. 111–126.

Gulliford, A.R., Flint, S.S., and Hodgson, D.M., 2017, Crevasse splay processes and deposits in an ancient distributive fluvial system: the lower Beaufort Group, South Africa: Sedimentary Geology, v. 358, p. 1–18.

Hajek, E.A., and Edmonds, D., 2014, Is river avulsion style controlled by floodplain morphodynamics?: Geology, v. 42, p. 199–202.

Huang, C., Wylie, B., Yang, L., Homer, C., and Zylstra, G., 2002, Derivation of a tasselled cap transformation based on Landsat 7 at-satellite reflectance: International Journal of Remote Sensing, v. 23, p. 1741–1748.

Jerolmack, D.J., and Mohrig, D., 2007, Conditions for branching in depositional rivers: Geology, v. 35, p. 463–466.

Jobe, Z.R., Howes, N.C., Straub, K.M., Cai, D., Deng, H., Laugier, F.J., Pettinga, L.A., and Shumaker, L.E., 2020, Comparing aggradation, superelevation, and avulsion frequency of submarine and fluvial channels: Frontiers in Earth Science, v. 8, doi:10.3389/feart.2020.0053.

Johnson, E.A., and Pierce, F.W., 1990, Variations in fluvial deposition on an alluvial plain: an example from the Tongue River Member of the Fort Union Formation (Paleocene), southeastern Powder River Basin, Wyoming, USA: Sedimentary Geology, v. 69, p. 21–36.

Johnston, G.H., David, S.R., and Edmonds, D.A., 2019, Connecting fluvial levee deposition to flood-basin hydrology: Journal of Geophysical Research: Earth Surface, v. 124, p. 1996–2012.

Jones, H., and Hajek, E.A., 2007, Characterizing avulsion stratigraphy in ancient alluvial deposits: Sedimentary Geology, v. 202, p. 124–137.

Jones, L.S., and Harper, J.T., 1998, Channel avulsions and related processes, and large-scale sedimentation patterns since 1875, Rio Grande, San Luis Valley, Colorado: Geological Society of America, Bulletin, v. 110, p. 411–421.

Jones, L., and Schumm, S., 1999, Causes of avulsion: an overview, *in* Smith, N.D., and Rogers, J., eds., Fluvial Sedimentology VI: International Association of Sedimentologists, Special Publication 28, p. 171–178.

Kauth, R.J., and Thomas, G., 1976, The tasselled cap: a graphic description of the spectral–temporal development of agricultural crops as seen by Landsat: Laboratory for Applications of Remote Sensing Symposia, v. 4B, p. 41–51.

Kraus, M.J., and Gwinn, B., 1997, Facies and facies architecture of Paleogene floodplain deposits, Willwood Formation, Bighorn basin, Wyoming, USA: Sedimentary Geology, v. 114, p. 33–54.

Kraus, M., Wells, T., Smith, N., and Rogers, J., 1999, Recognizing avulsion deposits in the ancient stratigraphical record, *in* Smith, N.D., and Rogers, J., eds., Fluvial Sedimentology VI: International Association of Sedimentologists, Special Publication 28, p. 251–268.

Kumar, R., 1993, Coalescence megafan: multistorey sandstone complex of the late-orogenic (Mio-Pliocene) sub-Himalayan belt, Dehra Dun, India: Sedimentary Geology, v. 85, p. 327–337.

Labourdette, R., and Jones, R.R., 2007, Characterization of fluvial architectural elements using a three-dimensional outcrop data set: Escanilla braided system, South-Central Pyrenees, Spain: Geosphere, v. 3, p. 422–434.

Lombardo, U., 2016, Alluvial plain dynamics in the southern Amazonian foreland basin: Earth System Dynamics, v. 7, p. 453–467.

Lombardo, U., 2017, River logjams cause frequent large-scale forest die-off events in southwestern Amazonia: Earth System Dynamics, v. 8, p. 565–575.

Louzada, R.O., Bergier, I., and Assine, M.L., 2020, Landscape changes in avulsive river systems: case study of Taquari River on Brazilian Pantanal wetlands: Science of the Total Environment, v. 723, no. 138067.

Makaske, B., Smith, D.G., and Berendsen, H.J., 2002, Avulsions, channel evolution and floodplain sedimentation rates of the anastomosing upper Columbia River, British Columbia, Canada: Sedimentology, v. 49, p. 1049–1071.

Makaske, B., Maathuis, B.H., Padovani, C.R., Stolker, C., Mosselman, E., and Jongman, R.H., 2012, Upstream and downstream controls of recent avulsions on the Taquari megafan, Pantanal, south-western Brazil: Earth Surface Processes and Landforms, v. 37, p. 1313–1326.

Mayewski, P.A., Rohling, E.E., Stager, J.C., Karlén, W., Maasch, K.A., Meeker, L.D., Meyerson, E.A., Gasse, F., van Kreveld, S., and Holmgren, K., 2004, Holocene climate variability: Quaternary Research, v. 62, p. 243–255.

McCarthy, T., Ellery, W., and Stanistreet, I., 1992, Avulsion mechanisms on the Okavango fan, Botswana: the control of a fluvial system by vegetation: Sedimentology, v. 39, p. 779–795.

Mitra, D., Tangri, A.K., and Singh, I.B., 2005, Channel avulsions of the Sarda river system, Ganga Plain: International Journal of Remote Sensing, v. 26, p. 929–936.

Mohrig, D., Heller, P.L., Paola, C., and Lyons, W.J., 2000, Interpreting avulsion process from ancient alluvial sequences: Guadalope–Matarranya system (northern Spain) and Wasatch Formation (western Colorado): Geological Society of America, Bulletin, v. 112, p. 1787–1803.

Morón, S., Amos, K., Edmonds, D.A., Payenberg, T., Sun, X., and Thyer, M., 2017, Avulsion triggering by El Niño–Southern Oscillation and tectonic forcing: the case of the tropical Magdalena River, Colombia: Geological Society of America, Bulletin, v. 129, p. 1300–1313.

Morozova, G., and Smith, N., 1999, Holocene avulsion history of the lower Saskatchewan fluvial system, Cumberland Marshes, Saskatchewan–Manitoba, Canada, *in* Smith, N.D., and Rogers, J., eds., Fluvial Sedimentology VI: International Association of Sedimentologists Special Publication 28, p. 231–249.

Morozova, G.S., and Smith, N.D., 2000, Holocene avulsion styles and sedimentation patterns of the Saskatchewan River, Cumberland Marshes, Canada: Sedimentary Geology, v. 130, p. 81–105.

Olsen, H., 1989, Sandstone-body structures and ephemeral stream processes in the Dinosaur Canyon Member, Moenave Formation (Lower Jurassic), Utah, USA: Sedimentary Geology, v. 61, p. 207–221.

Perez-Arlucea, M., and Smith, N.D., 1999, Depositional patterns following the 1870s avulsion of the Saskatchewan River (Cumberland Marshes, Saskatchewan, Canada): Journal of Sedimentary Research, v. 69, p. 62–73.

Platt, N.H., and Keller, B., 1992, Distal alluvial deposits in a foreland basin setting: the Lower Freshwater Miocene), Switzerland: sedimentology, architecture and palaeosols: Sedimentology, v. 39, p. 545–565.

Poore, R., Dowsett, H., Verardo, S., and Quinn, T.M., 2003, Millennial-to century-scale variability in Gulf of Mexico Holocene climate records: Paleoceanography, v. 18, no. 1048.

Porsani, J.L., Assine, M.L., and Moutinho, L., 2005, Application of GPR in the study of a modern alluvial megafan: the case of the Taquari River in Pantanal Wetland, west-central Brazil: Subsurface Sensing Technologies and Applications, v. 6, p. 219–233.

Richards, K., Chandra, S., and Friend, P., 1993, Avulsive channel systems: characteristics and examples, *in* Best, J.L., and Bristow, C.S., eds., Braided Rivers: Geological Society of London, Special Publications 75, p. 195–203.

Sinha, R., 2008, Kosi: rising waters, dynamic channels and human disasters: Economic Political Weekly, v. 43, p. 42–46.

Sinha, R., 2009, The great avulsion of Kosi on 18 August 2008: Current Science, v. 97, p. 429–433.

Slingerland, R., and Smith, N.D., 1998, Necessary conditions for a meandering-river avulsion: Geology, v. 26, p. 435–438.

Slingerland, R., and Smith, N.D., 2004, River avulsions and their deposits: Annual Review of Earth and Planetary Sciences, v. 32, p. 257–285.

Smith, N.D., Cross, T.A., Dufficy, J.P., and Clough, S.R., 1989, Anatomy of an avulsion: Sedimentology, v. 36, p. 1–23.

Smith, N.D., and Perez-Arlucea, M., 1994, Fine-grained splay deposition in the avulsion belt of the lower Saskatchewan River, Canada: Journal of Sedimentary Research, v. 64, p. 159–168.

Stouthamer, E., 2001, Sedimentary products of avulsions in the Holocene Rhine–Meuse Delta, the Netherlands: Sedimentary Geology, v. 145, p. 73–92.

Stouthamer, E., and Berendsen, H.J., 2001, Avulsion frequency, avulsion duration, and interavulsion period of Holocene channel belts in the Rhine–Meuse delta, the Netherlands: Journal of Sedimentary Research, v. 71, p. 589–598.

Törnqvist, T.E., and Bridge, J.S., 2002, Spatial variation of overbank aggradation rate and its influence on avulsion frequency: Sedimentology, v. 49, p. 891–905.

Trigg, M.A., Bates, P.D., Wilson, M.D., Schumann, G., and Baugh, C., 2012, Floodplain channel morphology and networks of the middle Amazon River: Water Resources Research, v. 48, no. W10504.

Tunbridge, I.P., 1981, Sandy high-energy flood sedimentation: some criteria for recognition, with an example from the Devonian of SW England: Sedimentary Geology, v. 28, p. 79–95.

Valenza, J.M., Edmonds, D., Hwang, T., and Roy, S., 2020, Downstream changes in river avulsion style are related to channel morphology: Nature Communications, v. 11, no. 2116.

van Toorenenburg, K.A., Donselaar, M.E., and Weltje, G.J., 2018, The life cycle of crevasse splays as a key mechanism in the aggradation of alluvial ridges and river avulsion: Earth Surface Processes and Landforms, v. 43, p. 2409–2420.

Weissmann, G., Hartley, A., Nichols, G., Scuderi, L., Olson, M., Buehler, H., and Banteah, R., 2010, Fluvial form in modern continental sedimentary basins: distributive fluvial systems: Geology, v. 38, p. 39–42.

Weissmann, G., Hartley, A., Scuderi, L., Nichols, G., Davidson, S., Owen, A., Atchley, S., Bhattacharyya, P., Chakraborty, T., and Ghosh, P., 2013, Prograding distributive fluvial systems: geomorphic models and ancient examples, *in* Driese, S.G., and Nordt, L.C., eds., New Frontiers in Paleopedology and Terrestrial Paleoclimatology: Paleosols and Soil Surface Analog Systems: SEPM, Special Publication 104, p. 131–147.

Xue, C., 1993, Historical changes in the Yellow River delta, China: Marine Geology, v. 113, p. 321–330.

Zani, H., and De Fátima Rossetti, D. 2012, Multitemporal Landsat data applied for deciphering a megafan in northern Amazonia: International Journal of Remote Sensing, v. 33, p. 6060–6075.

Zani, H., Assine, M.L., and McGlue, M.M., 2012, Remote sensing analysis of depositional landforms in alluvial settings: method development and application to the Taquari megafan, Pantanal (Brazil): Geomorphology, v. 161, p. 82–92.

Received 15 April 2021; accepted 27 February 2022.